Synthesizing Vehicle Cornering Modes for Energy Consumption Analysis

Craig Steven Fedor

Thesis submitted to the faculty of the Virginia Polytechnic Institute and State University in partial fulfillment of the requirements for the degree of

Master of Science

In

Mechanical Engineering

Douglas J. Nelson, Chair

Hesham A. Rakha

Alexander Leonessa

April 30th, 2018

Blacksburg, Virginia

Keywords: battery electric vehicle, cornering, road curves, energy consumption, lateral acceleration, eco-routing

Synthesizing Vehicle Cornering Modes for Energy Consumption Analysis

Craig Steven Fedor

Academic Abstract

Automotive vehicle manufacturers have been facing increased pressures from legislative bodies and consumers to reduce the fuel consumption and greenhouse gas emissions (GHG) of new vehicles because of recent research showing the detrimental effects that these GHG emissions have on the environment. These pressures are encouraging manufactures and researchers to invest billions of dollars into the development of new advanced vehicle technologies. These investments have resulted in substantial progress in powertrain technologies that have led to the preliminary adoption of battery electric vehicles (BEV) and plug in hybrid electric vehicles (PHEV). Other areas of research are actively working to reduce the energy consumption of a vehicle regardless of its powertrain, through influencing the operator driving behaviors and optimizing the vehicle path. Research has shown that solely changing the way a vehicle is driven can reduce fuel consumption by 10-20%.

To effectively implement technologies like vehicle path optimization, an accurate method for predetermining vehicle energy expenditure along a given route before it is driven needs to be determined. Traditional methods involve finding energy use along each stretch of road in a network with either large-scale driving studies with instrumented vehicles or powerful computer road network simulation tools. These methods can prove costly and time consuming. Individual vehicle predictive energy estimation eliminates the need for costly energy consumption data acquisition or generation by utilizing vehicle velocity synthesizing techniques and vehicle powertrain models. Estimation of individual vehicle energy consumption along a route is done by identifying an origin-destination pair, detecting required full-stops along the path, and synthesizing multiple stop-to-stop velocity modes between each set of stops. The resulting velocity profile is paired with a vehicle powertrain model. A drawback of this individual synthesis technique is that the route is assumed to be one-dimensional and lacks inclusion of road curves and their associated velocity changes to maintain passenger comfort while cornering.

This thesis evaluates the merit of including or excluding road curves in vehicle energy consumption analysis and presents technique for modeling common road corners that require velocity changes to limit maximum lateral acceleration with limited inputs. The resulting corner synthesis method is combined with a validated vehicle powertrain model to complete full route consumption modeling. Two routes, an urban and highway, are modeled and driven to evaluate the accuracy of the full simulation model when compared with on-road data. The results show that corners can largely be ignored during vehicle energy consumption analyses along highway routes. The cornering effects on a vehicle during urban driving, however, should be considered in urban route analyses with multiple road curves. Inclusion of the cornering effects during an example urban route analysis reduced the consumption estimate error between the simulation and the on-road data from 5.7% to 1.7%.

Synthesizing Vehicle Cornering Modes for Energy Consumption Analysis

Craig Steven Fedor

General Audience Abstract

Automotive vehicle manufacturers have been facing increased pressures from legislative bodies and consumers to reduce the fuel consumption and harmful emissions of their newly produced vehicles as a result of new research showing the detrimental effects these emissions have on the environment. These pressures are encouraging manufactures and researchers to invest billions of dollars into the development of new advanced vehicle technologies. Some of these investments have resulted in substantial progress in powertrain technologies that have led to the preliminary adoption of electrified powertrain vehicles. Other areas of research are actively working to reduce the energy consumption of a vehicle, regardless of its powertrain, by influencing driver behavior and by optimizing the way a vehicle travels between an origin and destination. This intelligent vehicle routing is done by analyzing a range of possible routes and selecting the route that consumes the least amount of fuel.

An accurate method for predetermining vehicle energy expenditure along a given route before it is driven is needed to effectively implement intelligent vehicle routing systems. One common method is the generation of a road network-wide database with energy use figures for each section of road. This method requires expensive experimentation trials or network simulation software. Individual-level vehicle predictive energy estimation eliminates the need for costly fuel use generation by utilizing vehicle velocity generation techniques and vehicle powertrain models. Estimation of individual vehicle energy consumption along a route is done by identifying an origin-destination pair, detecting required full-stops along the path, and synthesizing multiple stop-to-stop velocity modes between each set of stops. The resulting velocity profile is paired with a specific vehicle powertrain model to determine fuel consumption. A drawback of this route generation technique is that the vehicle path is assumed to be one-dimensional and lacks inclusion of road curves and their associated velocity changes to maintain passenger comfort.

This thesis evaluates the merit of discounting road curves in predictive vehicle energy consumption analyses and presents a technique for modeling common road corners that require velocity changes to limit passenger discomfort. The resulting corner synthesis method is combined with a validated vehicle powertrain model to complete full route consumption modeling. Two routes, an urban and highway, are modeled and driven to evaluate the accuracy of the full simulation model when compared with on-road data. The results show that corners can largely be ignored during energy consumption analysis for highways. The cornering effects on a vehicle during urban driving, however, should be included in urban route analyses with multiple road curves. Inclusion of the cornering effects during an example urban route analysis decreased the error between the on-road consumption data and the simulation results.

Acknowledgements

I would like to thank all of the team members I have had the pleasure of working with over the last three years during my involvement with the Hybrid Electric Vehicle Team at Virginia Tech. I have learned more during this short time working on EcoCAR 3 than I ever thought possible.

I am forever in debt to Sam Reinsel for his thankless volunteering of his baby (the 2013 Chevrolet Volt). Thank you to Matt Moniot who provided the high-quality groundwork of this thesis and for always providing a helping hand. I would like thank Dr. Nelson for his continued dedication to his students and our passions. He continued to challenge me every week and truly made this masters experience enjoyable. I would certainly have not chosen this path had it not been for his unwavering commitment to education and research.

I would like to thank my wonderful and supportive family. I also cannot thank Emily enough for dealing with my multiple all-nighters in the lab with a smile on her face.

Table of Contents

List of Figures

List of Tables

List of Terms and Abbreviations

Battery Electric Vehicle	BEV
Internal Combustion Engine Vehicle	ICEV
Highway Fuel Economy Test	HwFET
Urban Dynamometer Drive Schedule	UDDS
Parallel Hybrid Electric Vehicle	PHEV
Greenhouse Gas	GHG
Global Positional System	GPS
Environmental Protection Agency	EPA
American Association of State Highway and Transportation Officials	AASHTO
Time to Lane Crossing	TLC
Extended Range Electric Vehicle	EREV
State of Charge	SOC
Controller Area Network	CAN

1 Thesis Introduction

There has been an increased emphasis in the transportation sector on reducing fuel use and greenhouse gas emissions (GHG) as more research has shown their detrimental effects on the environment and our health. According to the Lancet Commission on Pollution and Health [1.1], nine million deaths were attributed to pollution from automobiles and industrial practices worldwide in 2015. Pressures from legislators and the public are forcing transportation sectors to invest billions of dollars into research and development of more fuel-efficient modes of transportation. One notable result of these investments is the rise of the electrified powertrain vehicle. Plug-in hybrid electric vehicles (PHEVs) and battery electric vehicles (BEVs) produce considerably less, or no, tailpipe CO2 emissions when compared to conventional internal combustion engine vehicles (ICEV). In addition to advanced powertrain vehicles, studies have shown that solely driving any type of vehicle in a more controlled and efficient manner will reduce energy consumption and GHG. This technique, also known as eco-driving, involves driving less aggressively, cruising at lower speeds, and limiting vehicle idle time. Preliminary research on the effects of eco-driving indicate that it can reduce fuel use by up to 15% [1.2]. Additionally, intelligently routing vehicles to drive the least energy intensive route between an origin-destination pair will save even more fuel without any physical powertrain modifications. Studies into the effects of intelligent vehicle routing, also known as eco-routing, show a potential decrease in fuel consumption of 3.3% to 9.3% [1.3].

To successfully implement eco-routing systems, the estimated energy consumption along an array of vehicle routes needs to be quickly and reliably determined before they are driven. This is commonly done with generation of a network wide database with energy use figures for each section of road. Energy use along road sections, or between nodes, is found with either large-scale on-road data collection experiments or with fuel use estimation software [1.3] [1.4] [1.5]. Utilizing individual route energy consumption estimation [1.6] without extensive knowledge of a route will eliminate the need for complex simulation tools or resource intensive on-road experimentation. Individual estimation of vehicle energy consumption along a route is done by identifying an origin-destination pair, detecting required full-stops and their associated conditions along the path, and synthesizing multiple stop-to-stop naturalistic velocity modes between each set of stops. The resulting velocity profile is then matched with corresponding road grade data, as road grade significantly affects vehicle energy consumption [1.7], and is used as an input to a backwards-facing powertrain model. The model is vehicle specific and validated with publicly available dynamometer consumption data. This process is iteratively run for each reasonable path between an origin-destination pair, and the least energy intensive route is chosen. There are some drawbacks, however, of this route synthesis technique. First, this method does not use current traffic conditions to evaluate route energy consumption. Secondly, the route is assumed to be one-dimensional and lacks inclusion of road curves and their associated velocity changes to maintain passenger comfort. A vehicle driving around a corner incurs a lateral acceleration on the passengers, shown in Figure 1-1. The driver limits the experienced lateral acceleration by decrease velocity around the corner as the lateral acceleration is a function of cornering velocity and corner radius.

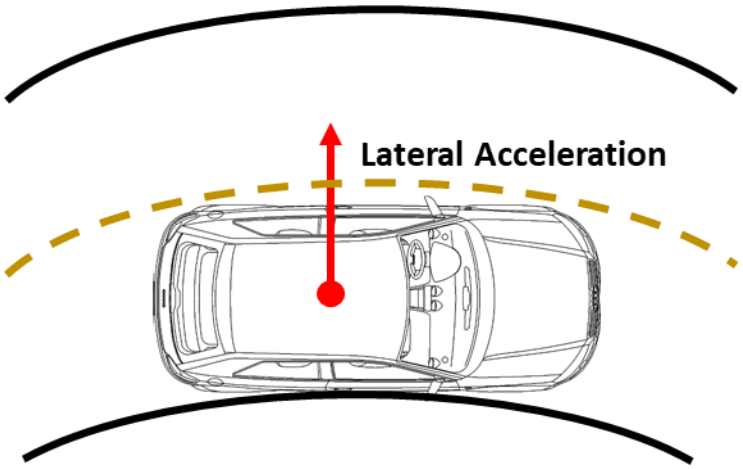

Figure 1-1: Lateral acceleration experienced by the vehicle and its passengers is a function of cornering velocity and corner radius.

This paper evaluates the merit of discounting the effect that road corners have on individual route energy consumption estimates. The first section introduces a method to generate velocity modes around road corners with a limited number of inputs. Then, vehicle routes with included cornering velocity segments are simulated with a validated backwards-facing powertrain model, and the results are used to identify the usefulness of modeling corners in preliminary route energy consumption models. Finally, road-testing with a BEV validates the road corner synthesis method and the powertrain model. This thesis is constructed with the intent of the main body acting as a publishable journal paper. For that reason, detailed sections describing methodologies and results deemed unnecessary for publication are found in the supplemental appendices.

1.1 Introduction References

[1.1] Philip, J. et al., The Lancet Commission on Pollution and Health, The Lancet, Volume 0, Issue 0 accessed Jan 28, 2018

[1.2] Fiat Group Automobiles, "Eco-driving Uncovered," Accessed April 2018, http://ecodrive.driveuconnect.eu/uploadedFiles/Fiatcouk/Stand_Alone_Sites/EcoDrive2010/en/ECO-DRIVING_UNCOVERED_summary_2010_EN.pdf

[1.3] Ahn, K. and Rakha, H., "Network-wide impacts of eco-routing strategies: A large-scale case study," Transportation Research D, vol. 25, pp. 119-130, Dec. 2013.

[1.4] Richter, M., Zinser, S., and Kabza, H., "Comparison of Eco and Time Efficient Routing of ICEVs, BEVs and PHEVs in Inner City Traffic," Vehicle Power and Propulsion Conference (VPPC), 2012 IEEE, Seoul, 2012, 1165-1169.

[1.5] Ericsson, E., Larsson, H., and Brundell-Freij, K., "Optimizing Route Choice for Lowest Fuel Consumption- Potential Effects of a New Driver Support Tool," Transportation Research Part C: Emerging Technologies 14(6):369-383, 2006.

[1.6] Warpe, H., Moniot, M., Nelson, D., and Baumann, W., "EcoRouting Strategy Using Variable Acceleration Rate Synthesis Methodology," SAE Technical Paper 2018-01-5005, 2018, doi:10.4271/2018-01-5005.

[1.7] Boriboonsomsin, K., and Barth, M., "Impacts of Road Grade on Fuel Consumption and Carbon Dioxide Emissions Evidenced by Use of Advanced Navigation Systems," Transportation Research Record. 2139, pp. 21-30. 10.3141/2139-03, 2009.

2 Journal Paper - Synthesizing Vehicle Cornering Modes for Energy Consumption Analysis

2.1 Abstract

Automotive vehicle manufacturers have been facing increased pressures from legislative bodies and consumers to reduce the fuel consumption and greenhouse gas emissions (GHG) of new vehicles. One area of research is actively working to reduce the energy consumption of a vehicle regardless of its powertrain by influencing the operator driving behaviors and optimizing the vehicle path. Research has shown that solely changing the way a vehicle is driven can significantly reduce vehicle fuel use.

To effectively implement technologies like vehicle path optimization, an accurate method for predetermining vehicle energy expenditure along a given route before it is driven is needed. Estimation of vehicle energy consumption along a route is done by identifying an origin-destination pair, detecting required full-stops along the path, and synthesizing multiple stop-to-stop velocity modes. A drawback of this synthesis technique is that the route is assumed to be one-dimensional and lacks inclusion of road curves and their associated velocity changes to maintain passenger comfort while cornering.

This paper evaluates the merit of including or excluding road curves in vehicle energy consumption analysis. The first section presents a technique for modeling common road corners that require velocity changes to limit maximum lateral acceleration with limited inputs. The resulting corner synthesis method is combined with a validated vehicle powertrain model to complete full route consumption modeling. Two example routes, an urban and highway, are modeled and driven by a test vehicle to evaluate the accuracy of the full simulation model when compared with on-road data. The results show that corners can largely be ignored during energy consumption analysis along highway routes. The cornering effects on a vehicle during urban driving, however, should be considered in urban route analysis with multiple road curves. Including the cornering effects during an example urban route analyses reduced the consumption estimate error between the simulation and the on-road data from 5.7% to 1.7%.

2.2 Introduction

Automotive vehicle manufacturers have faced increased pressures from legislative bodies and consumers to reduce the fuel consumption and GHG emissions of new vehicles. These pressures stem from new research showing the detrimental effects these harmful emissions have on the environment and are encouraging manufactures and researchers to invest billions of dollars into the development of new advanced vehicle technologies. Powertrain technologies have advanced significantly, and this has led to the preliminary consumer adoption of BEVs and PHEVs. Other areas of research are actively working to reduce the energy consumption of vehicles, regardless of its specific powertrain, by influencing the operator driving behavior and optimizing the vehicle routing path. On-the-fly vehicle path optimization is increasing in popularity due to recent advancements in the capabilities of on-board vehicle routing systems. Modern vehicle GPS guidance systems can monitor traffic information in real time and calculate a vehicle path that minimizes total travel time or travel distance in seconds. New research studying a third optimization criterion of minimizing vehicle energy consumption, referred to as eco-routing, has shown promising results. A preliminary analysis of a city-wide vehicle network using eco-routing optimization showed a fuel use reduction between 3.3% and 9.3% [2.1].

Many industries will benefit from the successful implementation of either fleet-wide or individual level eco-routing. Systematically minimizing energy use along the routes of mail and package delivery service providers will eliminate fleet fuel waste and reduce overhead costs. The main challenge of implementing

vehicle path optimization techniques is generating a reliable estimation of energy consumption over a given route before it has been driven. [2.1], [2.2], and [2.3] implementing eco-routing successfully, but with experimentally derived or simulated network-wide consumption data. The experimental methods require expensive, large-scale trials and hundreds of man-hours to collect road network consumption results. Constraining eco-routing possibilities to networks that only have empirical or simulation consumption data for a specific vehicle significantly reduces the usefulness of a system. An ideal eco-routing system will be able to estimate energy consumption over a completely unknown route. Accurate vehicle path energy use begins with synthesizing velocity profiles that closely resemble common driving behavior. Research by [2.4] on the ability to generate stop-to-stop velocity route profiles when given limited knowledge of a route is a promising method; however, this model ignores road corners and their effect on aggregate energy use. Accurate methods for predicting energy use with minimal knowledge of a route will expand the usefulness of eco-routing implementation. This paper analyzes whether including or excluding the effects of cornering into route synthesizing methods will increase modeling fidelity. First, this paper develops a corner velocity mode synthesis technique that requires minimal inputs with the use of experimentally derived parameters. In the next section, the generated curve modes are paired with a validated vehicle powertrain model to simulate on-road routes. These simulated routes were tested in a 2013 Chevrolet Volt to compare the simulation energy consumption results against the on-road testing data.

2.3 Previous Work

One common way to estimate fuel use along a route for eco-routing purposes is to utilize experimentally derived consumption figures from the large-scale driving studies in [2.3]. In these studies, participants are asked to drive around a road network with instrumented vehicles to determine the average fuel consumption between each network node pair--typically road intersections. The route fuel consumption for a vehicle traveling from an origin to a destination within the road network is simply the sum of fuel consumption between each specific node pair travelled. Finding consumption figures is trivial after the on-road experimental trials; however, these trials are expensive and time consuming to conduct. Powerful vehicle road network computer simulation software is another common method for route energy consumption estimation in [2.1] and [2.2].

Individual vehicle energy consumption analysis can also be conducted without preliminary road network analysis and limited road knowledge. Route characteristics known before individual energy use estimations are: route speed limits, road grade data, stop sign and traffic light locations, and route corner quantities and parameters. Stop signs and traffic lights have a significant effect on the energy consumption of a travelled route, as each encounter requires an energy intensive deceleration and acceleration event. [2.5] utilizes mandatory and conditional stop nodes in their eco-routing analysis. A mandatory stop node, like a stop sign, requires the vehicle to decelerate to a complete stop and assigns a predetermined time penalty. A conditional node, like a stop light that could be either green or red, is binary: it is either treated as a mandatory stop node or ignored completely. The route analysis in [2.5] is conducted twice when conditional nodes are present. Once treating conditional nodes as mandatory to obtain the worst-case energy use, and again when they are ignored for the best-case outcome. Other unknown variables, such as weather conditions and traffic congestion, quickly expand the required knowledge of a route and increase the computing power required for analysis. While road speed limits and grade data are publicly available, reliable historical traffic data is more difficult to obtain with limited resources. In addition, research studying the effects of traffic congestion on fuel consumption of advanced powertrain vehicles indicates the influence of traffic is not consistent across all types of vehicle powertrains. [2.6] shows that BEVs consume less energy, when compared to highway driving, in congested traffic down to speeds of 20-30 mph, under which BEV energy consumption begins to increase. ICEVs do not see a decrease in fuel economy in heavy traffic until congestion slows to 30 mph or less. The lack of conclusive results about the positive or negative effect of

roadway congestion on fuel use combined with the difficulty in obtaining reliable traffic data leads to the exclusion of the effect of traffic flow on route consumption in this paper.

An analysis of the energy consumption of a vehicle as it travels between an origin-destination pair begins with the generation of a vehicle velocity profile. Predetermining route energy consumption requires accurate modeling of vehicle velocity paths, or modes, with limited inputs. A basic method that models vehicle longitudinal acceleration and deceleration from rest to cruise velocity, and back down to rest, is called the trapezoid model. The model has three regions: a constant acceleration, zero acceleration, and a constant deceleration. This modeling method is elementary and straightforward to implement but offers significant room for improvement. This model is not indicative of real-world vehicle behavior as a step acceleration or deceleration input will result in an infinite longitudinal jerk pulse. [2.4] modified the trapezoid model to more closely represent natural driving and eliminate the acceleration step function. The synthesis model uses the driver maximum acceleration, or aggressiveness, and a constant jerk rate that results in a linearly increasing and decreasing acceleration. Referred to as the hill model, this more accurately represents actual human behavior that is not captured in the trapezoid model. When compared with the EPA Federal Test drive cycles, the hill model generation technique produces a synthesized route with a tractive energy error of less than 5% for the limited number of cases studied. This simplified mode synthesis technique is promising for the development of a simplified corner generation technique that still closely matches natural driver behavior with limited preliminary information.

A downside of the hill modeling technique is the lack of integration of cornering effects on energy consumption. Cornering effects on vehicle aggregate energy use are widely considered insignificant and the EPA does not consider cornering as influential on new vehicle efficiency assessments. This lack of integration into standardized tests in part stems from the inability to easily replicate corner events on a chassis dynamometer; however, there is still limited, if any, research into the quantitative impacts of ignoring cornering for energy consumption estimates. Figure 2-1 shows an analysis of vehicle fuel use data over 700,000 road miles by [2.7]. This empirical data indicates a preliminary connection to cornering effects and increased vehicle energy consumption.

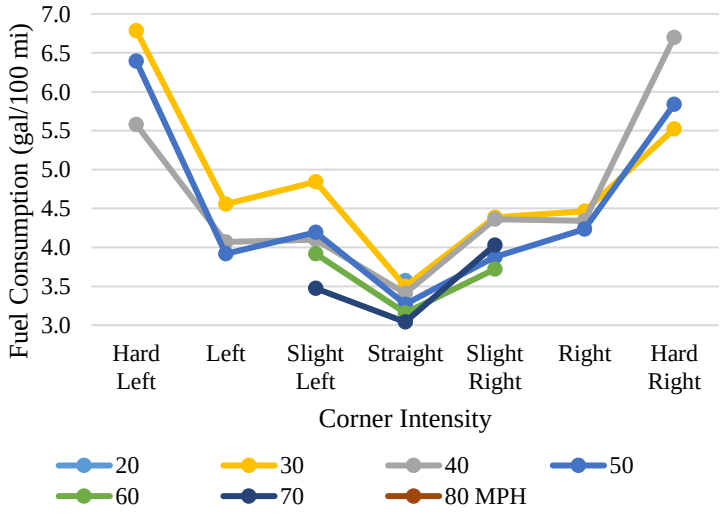

Figure 2-1: Changes in fuel consumption as a function of cornering intensity from [2.7]. The turn severity is defined as: straight < 10°, 10° < slight left/right < 80°, 80° < left/right < 100°, 100° < hard left/right < 180°.

2.4 Synthesizing Road Corner Modes

Surrounding environments (urban, rural, highway), roadway speed limits, and municipality guidelines are all factors that influence the physical characteristics of a corner [2.8]. Highways have corner banking to increase the velocity at which they can be safely navigated. Although there are multiple small characteristics that differentiate road curves from one another, only two basic properties effectively describe them for analysis: the corner angle and the corner radius. The corner angle is the "sweep" of the curve in degrees or radians, and the corner radius is the distance from the corner arc to its center in meters (Figure 2-2). To avoid discontinuity on straight segments where corner radius is infinite, curvature k, defined as

$$k = \frac{1}{R} \qquad \text{Equation 2-1}$$

where R is corner radius, is used to describe the magnitude of a road curve.

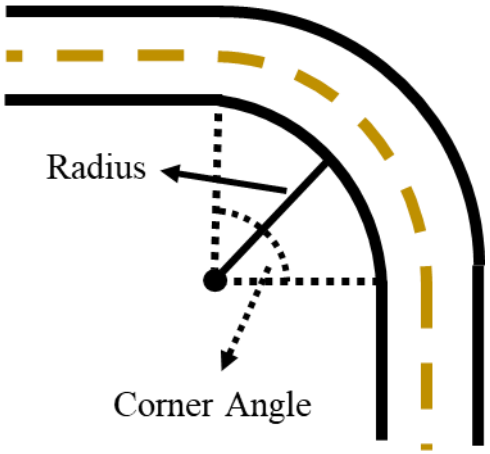

Figure 2-2: Simplified diagram of a road corner with the two characteristics of corner angle and radius.

The availability of open-source GPS road data makes finding curve properties simple when compared to previous methods, which required either a team of surveyors or detailed road map analysis. Analyzing public GPS road information to obtain road curvature and angle data is straightforward, as [2.9] accurately classified the constant curvature and type of horizontal curves with 90.1% accuracy by analyzing GPS data. There are drawbacks, however, to oversimplifying road corners as having a constant curvature. Vehicle trajectory around a constant curvature turn incurs a lateral acceleration step profile when transitioning between a straight road segment, with a curvature of zero, to a segment with a constant curvature. This lateral acceleration step profile results in an infinite lateral jerk,

$$J_{lat} = \frac{\partial a_{lat}}{\partial t} \qquad \text{Equation 2-2}$$

where a_{lat} is lateral acceleration in m/s^2 and t is time in seconds. The lateral acceleration in a curve is

$$a_{lat} = kV_t^{\,2} \qquad \text{Equation 2-3}$$

where V_t is the cornering velocity. Similar to the trapezoid model, this infinite jerk is not indicative of real-world vehicle control. A transitionary period between tangent straight road segments and a constant curvature corner is required to more accurately model real-world driving behavior.

2.4.1 9-Region Corner Mode Generation

There are many ways to incorporate a transitionary period into a vehicle path before and after a constant curve corner, but the most common is the clothoid curve [2.10]. The clothoid, also known as an Euler spiral, effectively models a vehicle trajectory in a curve. A clothoid has a curvature that increases as a linear function of the traveled curved distance. The linear curvature transition emulates the constant steering input that eases a vehicle in and out of a curve. Several assumptions must be met in order to use the clothoid to estimate vehicle transition into a corner. First, it is assumed that the vehicle travels around the corner at a constant velocity. In real-world scenarios, this is not usually the case--drivers tend to decelerate before corners but also continue slowing down well into the turn. This technique is not recommended because inducing multiple forces on a tire, cornering and tractive, at the same time can incur an unpredictable tire response. The ideal case is that a vehicle fully decelerates to match the predetermined turning velocity, V_t, required to maintain a maximum lateral acceleration before cornering begins. This assumption also removes another layer of humanistic behavior from the turn synthesis. The deceleration and acceleration profiles that transition the vehicle from cruise velocity to cornering velocity are developed from the hill model in [2.4]. Secondly, the input steering rate of the vehicle is increasing at a constant value. Lastly, the vehicle is mathematically represented by the bicycle model with the Ackermann steering effect assumed to be insignificant; this will be addressed later in this paper. If these three assumptions are met and maintained, a clothoid transition period accurately maps the vehicle path around a corner [2.11].

[2.12] derives the clothoid transition segment equations from the Fresnel integral, giving the resulting curvature as a function of distance traveled along the clothoid curve as

$$k(s) = 2c^2 s, \qquad \text{Equation 2-4}$$

where c is a constant describing the clothoid shape, and s is the distance along the curve. The curvature as a function of distance is converted into a function of time, as the powertrain model used in this analysis uses time and velocity as the model inputs, not time and distance. The powertrain model input constraint requires adaptation of the distanced-based constant, c, to a time-based constant. The conversion is

$$Er = 2c^2 V_t, \qquad \text{Equation 2-5}$$

resulting in the curvature as a function of time,

$$k = E_r t_E, \qquad \text{Equation 2-6}$$

where E_r is the easement rate and t_E is the curvature transition time. The easement rate is related to curvature and transition time as

$$E_r = \frac{\partial k}{\partial t}, \text{ or} \qquad \text{Equation 2-7}$$

$$E_r = \frac{k}{t_E}. \qquad \text{Equation 2-8}$$

This method only requires two additional corner model inputs, curve entry and curve exit times. These two inputs are further reduced to one, as idealized driving will consist of equal transition times for curve exit and entry. The entry and exit times correspond to the driver specific easement rate.

Figure 2-3 and Figure 2-4 are the overhead view corner perspective and velocity profile of the resulting 9-region piecewise curve, respectively. The 9-region curve is constructed with two clothoids, R4 and R6, and a constant radius curve, R5. The clothoid segments have a linearly increasing and decreasing curvature, shown in Figure 2-6 compared to the constant corner curvature. The constant curvature segment is

shortened or lengthened to account for the turn angle of the corner. The regions outside the curve are the longitudinal deceleration, R1, 2, 3, and acceleration, R7, 8, 9, events described by the hill model in [2.4]. This 9-region model is referred to as the clothoid model in the remainder of this paper. The piecewise definitions of curvature in each region of the turn are,

$$k(t_r) = \begin{cases} R1,2,3: 0 \\ R4: E_r t_r \\ R5: k \\ R6: k - E_r t_r \\ R7,8,9: 0 \end{cases} \quad \text{Equation 2-9}$$

where t_r is the region time that resets to zero at the beginning of each region independent of the global event time t_g.

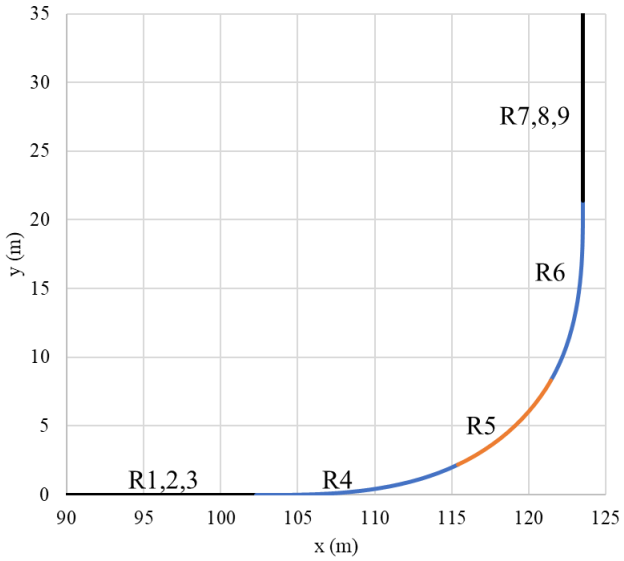

Figure 2-3: Resulting overhead view of the 9-region clothoid model corner with annotated regions.

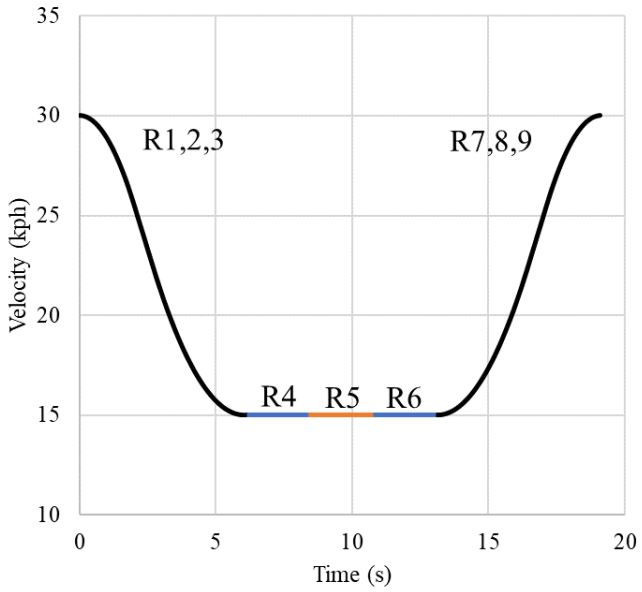

Figure 2-4: Resulting velocity profile of the 9-region clothoid model corner with annotated regions.

Figure 2-5 depicts the clothoid model compared to a curve with only a constant curve segment. The two corners have the same angle of turn and constant radius. Due to the relationship between corner curvature and lateral acceleration, the linear increase of curvature directly correlates to a linear increase of lateral acceleration (Figure 2-6). This eliminates the unnatural lateral jerk pulse experienced in a constant curvature corner.

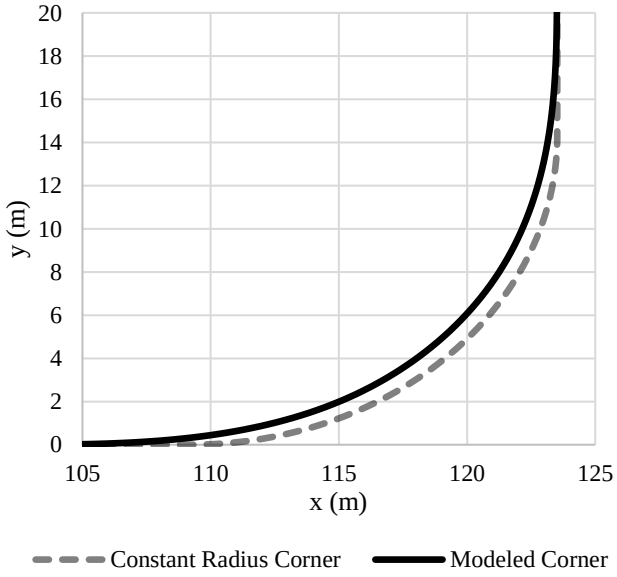

Figure 2-5: Resulting overhead view of the 9-region clothoid model corner compared with the constant radius corner

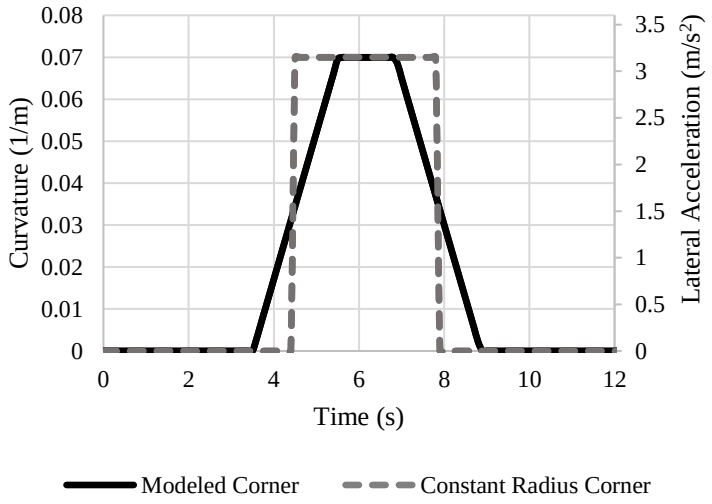

Figure 2-6: Curvature and lateral acceleration vs time of the 9-region clothoid model corner contrasted with the constant radius corner

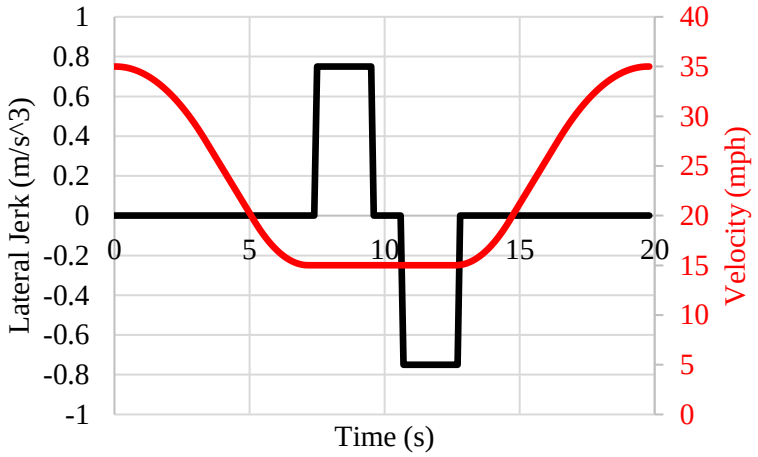

Figure 2-7: Lateral jerk against the velocity trace of the vehicle through a corner. Note the vehicle reaches cornering velocity before any lateral events occur.

The longitudinal accelerations that result from changing vehicle velocity to safely navigate the curve and lateral accelerations experienced in the curve are isolated in this model to avoid modeling improper driving behavior. The deceleration and acceleration events fully take place on straight road segments before and after the corner (Figure 2-8). Overlapping longitudinal and lateral accelerations, shown in Figure 2-9, result in a parabolically changing resultant acceleration vector magnitude,

$$a_{resultant} = \sqrt{a_{lat}^2 + a_{long}^2}\,, \qquad \text{Equation 2-10}$$

that causes unusual tire loading and uncomfortable motion for passengers. This also results in a linearly changing jerk value that has a non-zero derivative, or snap. Snap is the 4th derivative of an object's position vector expressed as

$$snap = \frac{dj}{dt}.$$ Equation 2-11

While there is limited research on snap and its effects, [2.13] cites that snap should be limited as much as possible to ensure maximum passenger comfort. This mathematically describes why slowing down while entering a corner is a subjectively uncomfortable experience for vehicle occupants. Ideally, a driver will decelerate and accelerate before initiating a cornering maneuver; therefore, this proper behavior is modeled in the corner route synthesis. It is important to note that combining cornering entry and exit and velocity change events decreases the total time to navigate the corner while still maintaining the same maximum acceleration as the isolated corner.

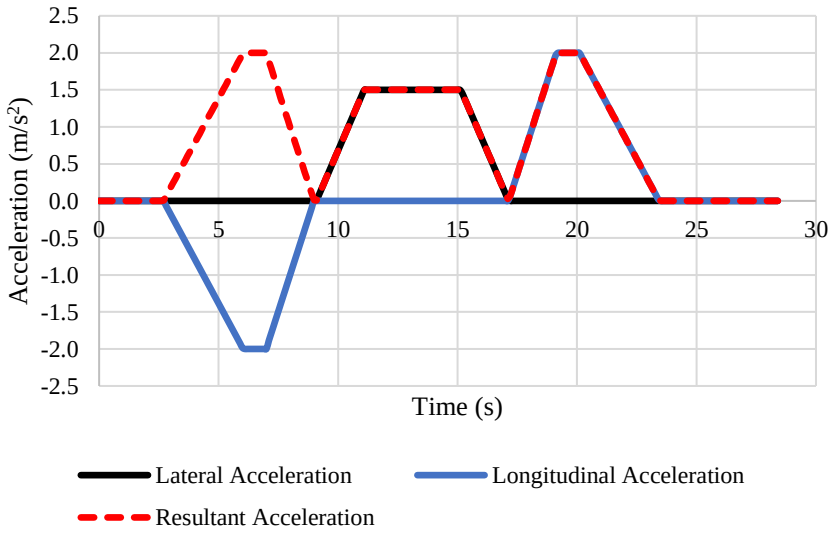

Figure 2-8: The resultant acceleration when initiating cornering after fully decelerating and finishing cornering before accelerating back to cruise velocity. Figure 2-4 is representative of the velocity profile of this event.

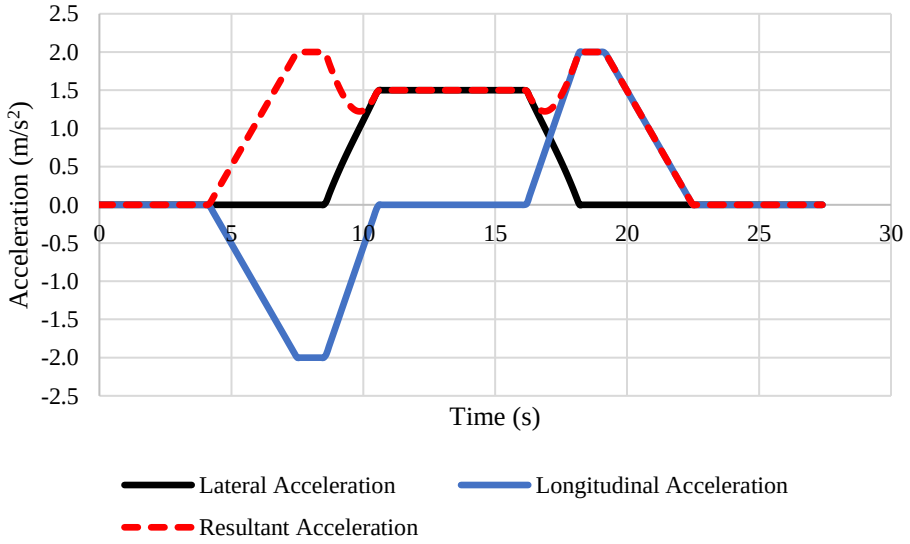

Figure 2-9: The resultant acceleration when initiating cornering while decelerating and accelerating out of a curve. The parabolic acceleration indicates a non-zero snap value. Figure 2-4 is representative of the

velocity profile of this event. This curve is also known as the 7-region curve and is discussed more the in the supplemental appendices.

The clothoid model has two physical curve inputs, constant corner curvature and corner angle, that are independent of the way the vehicle is driven. Easement rate is the driver dependent variable that corresponds to curve transition time, t_E. The easement rate is a subjective parameter, as no two drivers will rotate the steering wheel at the same rate when entering a turn. The easement rate is tuned to represent a wide range of drivers by finding the average transition time of entering and exiting a curve by utilizing on-road experimentation. A 2013 Chevrolet Volt was instrumented with angular rate sensors and accelerometers to experimentally determine an average easement time for a wide array of curve cases. The ease in and out times were found using two different drivers to collect a more generalized sample. Data collection was conducted on urban roads in Blacksburg, Virginia, USA with a wide range of unique road curves. Data from the angular rate sensors correlate to an average corner entry and exit time of approximately two seconds. Figure 2-10 is a histogram of the experimental turn transition times derived from the angular rate sensors with the normal distribution projected over it, and Figure 2-11 is the velocity at which the specified easement time occurred, which shows there is a weak correlation between vehicle corner velocity and easement time.

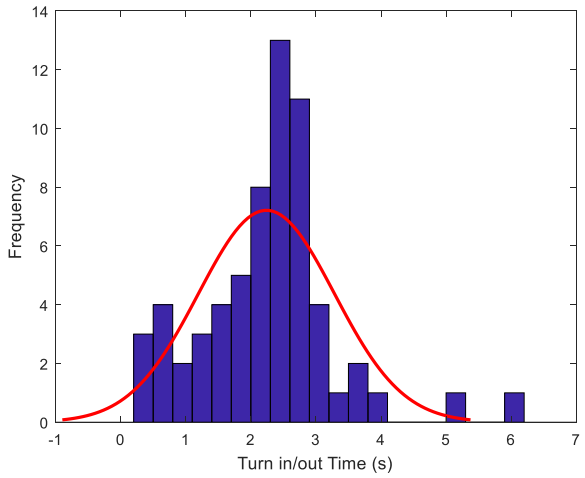

Figure 2-10: Histogram of the corner entry and exit times obtained from on-road testing with a 2013 Chevrolet Volt.

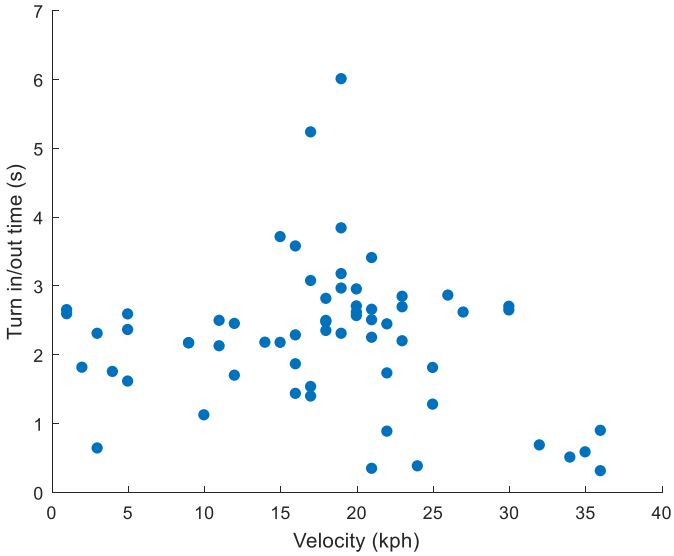

Figure 2-11: Distribution of the easement times across differing velocities indicating easement time and vehicle turn velocity are not strongly influenced by one another.

2.4.2 Cornering Velocity Derivation

Passenger comfort is the dominant metric behind a driver's estimation of the speed at which they will navigate a turn. Under normal operating conditions, modern passenger vehicle tires rarely encounter cornering speeds that push them beyond their frictional limits. This is also known as the nonlinear control region. Reducing velocity around corners and limiting lateral acceleration provides safer and more comfortable travel. Studies by [2.14] and [2.15] found that chosen vehicle cornering velocity is a function of lane width, the driver's preexisting familiarity of the curve, and non-curve cruising velocity. [2.15] used the metric time to lane crossing (TLC) to analyze the decision structure of how fast a driver chooses to navigate a corner. TLC is defined as the time necessary for the vehicle to reach the inner or outer lane edge if the steering and throttle controls were held constant. Drivers subconsciously maintain a TLC through a curve that gives them a buffer to adjust their course if an obstacle were to arise. By determining that the TLC is a function of the driver anticipated steering error, [2.15] developed a two-region envelope of maximum lateral acceleration as a function of cornering velocity. Figure 2-12 contains the resulting maximum lateral acceleration envelope for a passenger vehicle as a function of vehicle corning velocity. The envelope has two distinct regions to capture behavior at low and high velocities. The low velocity region below 18 kph is defined as

$$A_{lat} \leq kV^2, \qquad \text{Equation 2-12}$$

and the high velocity region above 18 kph is defined as

$$A_{lat} \leq A_{latmax} - \Delta C_{max} V^2, \qquad \text{Equation 2-13}$$

where A_{latmax} is the maximum lateral acceleration the specific driver is willing to experience, and ΔC_{max} is the maximum path curvature variation. For example, a driver with previous knowledge of the upcoming curves would have a ΔC_{max} value of 2 km^{-1} while an inexperienced driver would have a ΔC_{max} value of 10 km^{-1} to maintain a larger safety margin. This envelope is tunable to a specific driver aggressiveness value by increasing the maximum lateral acceleration term. This value sets the acceleration "peak" experienced around 20 kph. For example, the peak lateral acceleration value the driver is willing to

experience in Figure 2-12 is 4.9 m/s^2 or 0.5g. Note that the envelope edge is the *maximum* lateral acceleration a driver would subject themselves to at a given velocity.

Driving at night, driving through inclement weather, or transporting other passengers are all factors that contribute to the driver keeping lateral accelerations much lower than the envelope upper limits. This lateral acceleration envelope is validated with the same data acquisition system that found the curve transition times. Conversion of the lateral acceleration in the envelope to curve radius produces a maximum curve radius for each velocity in Figure 2-13. The curve in Figure 2-13 ends at 15 kph, as common road corners will not require deceleration below that velocity.

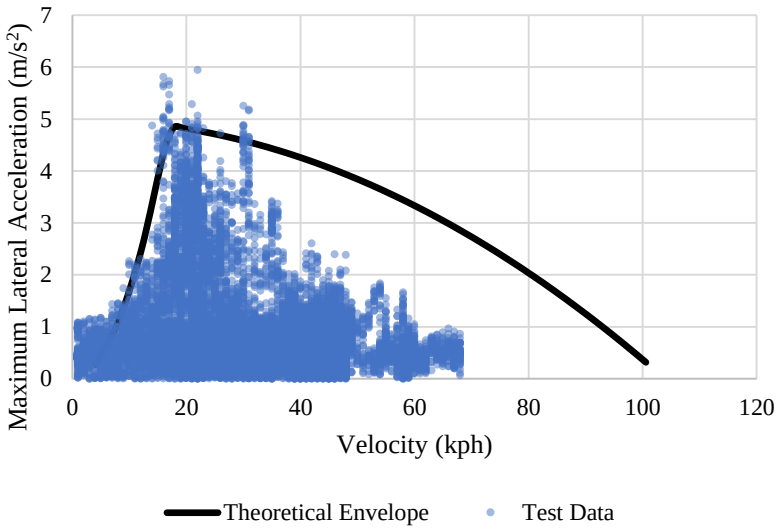

Figure 2-12: Lateral acceleration envelope from [2.15] with overlaid experimental data acquired with a 2013 Chevrolet Volt.

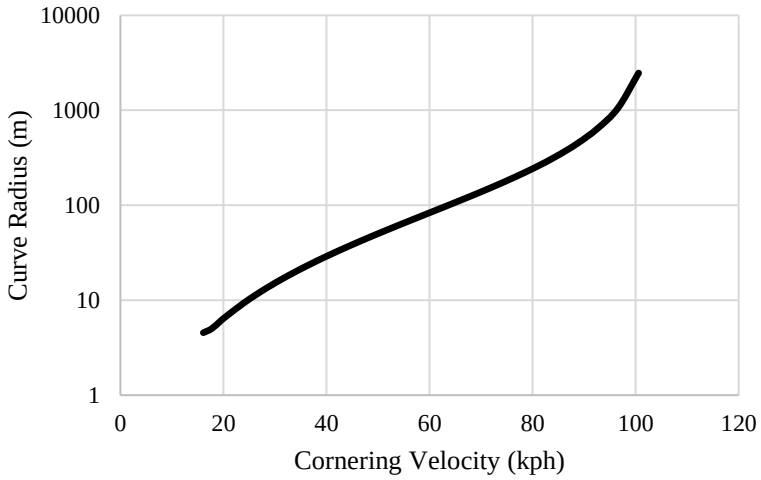

Figure 2-13: Maximum curve radius for a cornering velocity to remian under the maximum acceleration limits in Figure 2-12. Note the logarithmic radius scale on the y-axis.

The longitudinal accelerations experienced while accelerating from cruise velocity to cornering velocity, or vice versa, are metrics that vary widely depending on the specific driver aggressiveness pattern. A study

on the accelerations experienced during normal, everyday driving concluded, like above, that vehicles are rarely driven at their operational and frictional limits [2.16]. The 50-percentile longitudinal acceleration and deceleration value of roughly 2 m/s^2 for city and arterial driving from [2.16] is used in the curve velocity profile synthesis.

Given a route segment with known corner parameters derived from GPS data, the above modeling technique will synthesize the vehicle deceleration from cruise velocity to the specified cornering velocity, model the forces experienced in the curve, and synthesize the acceleration back to cruise velocity. The lateral and longitudinal accelerations experienced are tuned to match a driver aggressiveness profile in order to more closely resemble real-world operation. The resulting velocity profile that envelopes the entire cornering event is used as the velocity-time input to a vehicle specific powertrain model that calculates the energy consumption.

2.5 Powertrain Model

An accurate powertrain model is essential for effectively predicting the energy consumption along a route. The powertrain model operates by starting with a prescribed velocity trace. The process is discrete, as the forces acting on the vehicle to match the velocity trace are calculated for each specific timestep. Through differentiation of these forces, the required powertrain power is found for each timestep. This modeling technique is also known as a backwards facing powertrain model, as the powertrain requirements come from the velocity trace as an input.

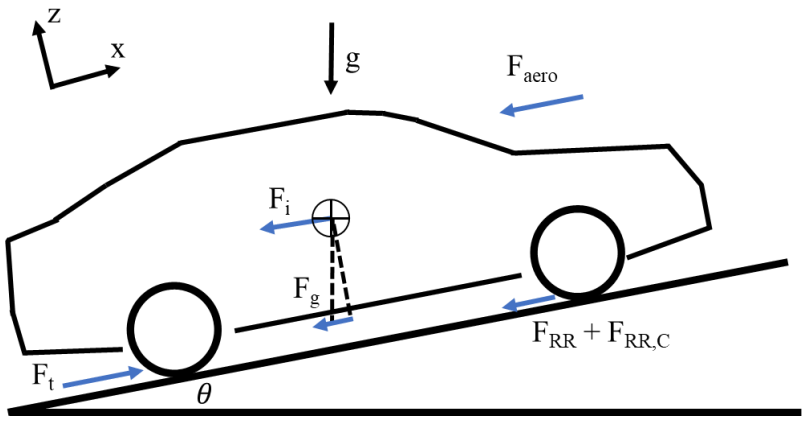

Figure 2-14: Free body diagram of a vehicle glider model driving through a corner

The forces acting on a vehicle are the fundamental building blocks of a powertrain model. The vehicle glider model simplifies the vehicle response to the environment by reducing the physical dynamics to six fundamental forces. The resulting force balance of the glider model free body diagram is

$$F_t = F_{aero} + F_g + F_{RR} + F_{RR,C} + F_i \qquad \text{Equation 2-14}$$

where:

F_t = wheel tractive force,

F_{aero} = aerodynamic drag force,

F_g = grade force,

F_{RR} = rolling resistance force,

$F_{RR,C}$ = cornering rolling resistance force,

F_i = inertial force.

The grade, aerodynamic drag, rolling resistance, and inertial forces are well studied and common in almost all vehicle dynamics problems. Cornering rolling resistance is the resistive force experienced by a vehicle during cornering due to tire deformation and slip angle. The cornering force is a function of vehicle cornering stiffness, or how compliant it is around a curve, and the lateral acceleration experienced during the corner. The equation is,

$$F_{RR,C} = \frac{m^2 a_{lat}^2}{2C_\alpha} \qquad \text{Equation 2-15}$$

where C_α is the vehicle cornering stiffness in N/rad, m is the test mass of the vehicle, and a_{lat} is the lateral acceleration experienced around the curve. The detailed vehicle dynamics derivation of the cornering force is in the supplemental appendices.

2.5.1 Powertrain Model Validation

Finding the total tractive energy at the wheels over a route with a time and velocity-based backwards-facing model is straightforward. Differentiating the vehicle velocity traces with respect to time yields the vehicle acceleration. The tractive force derived from the glider model equations multiplied by velocity results in the required power at the wheels. Integrating this value gives the overall tractive energy of a route. Using tractive energy at the wheels is sufficient in estimating non-powertrain specific energy use along a route; however, it does not factor driveline loss, powertrain efficiency, or the control strategy into the total energy use estimations. Most notably, this technique disregards vehicle and powertrain inefficiency such as driveline friction, engine or motor losses, and accessory loads (e.g. HVAC and lighting). With a desired increase in fidelity of energy consumption models comes the difficulty of obtaining more vehicle-specific powertrain parameters. [2.17] and [2.18] developed this powertrain model for use with ICEVs, PHEVs, and BEVs. This discrete backwards-facing model handles velocity and time traces as inputs and generates vehicle energy consumption and power demand as the output. Publicly available dynamometer test data from [2.19] is used to validate the powertrain model for specific vehicles. Scaling and tuning model input parameters matches the model results with dynamometer testing data.

The vehicle used during the on-road energy consumption testing was a stock 2013 Chevrolet Volt. The Volt is an extended range electric vehicle (EREV) which utilizes one internal combustion engine and two electric motors for propulsion. [2.20] provides the details of this specific Voltec propulsion system. The Volt travels an EPA-labeled 38 miles on battery power before the ICE turns on to maintain the battery state of charge (SOC). The on-road testing is conducted during this all-electric operation, or charge depleting (CD), window. This allows the Volt to be modeled as a short-range BEV, eliminating the complexities of modeling a complete hybrid powertrain. This corner synthesis analysis uses a BEV because they have predictable control strategies (no multispeed transmission shift maps to model) and there are large amounts of publicly available chassis dynamometer consumption data.

The 2013 Chevrolet Volt powertrain model is adjusted to most closely match chassis dynamometer results from [2.19] by scaling electric motor loss coefficients, adjusting the accessory power load, and modifying the regenerative braking fraction. The iterative tuning process produces a model with an energy use estimation error of +/- 2% for the common drive cycles in Table 2-1 that envelop common driving styles and scenarios. The modeled drive profiles are the 0-80-0 mph (0-129-0 kph) steady state speed steps cycle, the Highway Fuel Economy Test cycle (HwFET), the US06 cycle, and the Urban Dynamometer Driving Schedule (UDDS). There is a 12% SOC error between the dynamometer results and the powertrain model

of the steady state speed steps schedule; however, this stems from discrepancies that develop at velocities higher than 70 mph. The steady state velocities are also isolated and modeled with no acceleration or decelerations to examine at which velocities the model begins to deviate from dynamometer results. The powertrain model has a minimal error when compared against dynamometer results and is a reliable method for predicting vehicle energy use. On-road testing further validates this powertrain model.

Table 2-1: 2013 Chevrolet Volt Model and dynamometer energy use results for different common drive cycles

	UDDS (Hot Start)	**HwFET**	**US06**	**0-80-0 SS**
Model Results [AC Wh/mi]	254.9	263.4	358.1	ΔSOC: 10.7 %
Dynamometer Results [AC Wh/mi]	253.6	261.0	364.0	ΔSOC: 9.5 %
Model Error [AC Wh/mi]	-1.3	-2.4	5.9	1.2 %
Percent deviation [%]	-0.53%	-0.90%	1.62%	12.6%

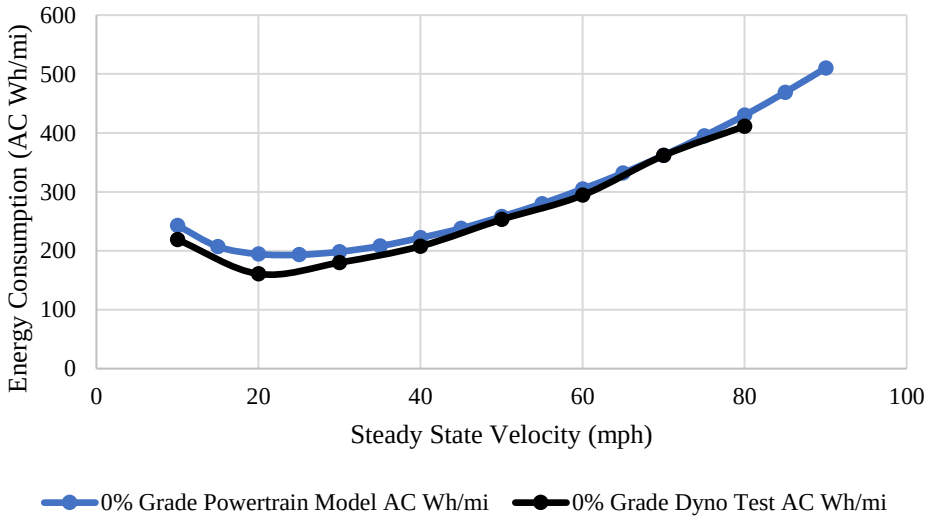

Figure 2-15: Modeled Volt steady state velocity consumption versus results from dynamometer testing.

2.6 Results

Combining the powertrain model with the previously derived cornering velocity profiles gives a reliable energy consumption estimate for a cornering event. Coupling the simulation results with the on-road test data reveals the benefits and shortcomings of the modeling and synthesis techniques.

2.6.1 Simulation Results

Analyzing the cornering force effect specifically during a corner isolates it from the inertial forces experienced while changing velocity. Using Figure 2-12 for lateral acceleration values, an analysis of a range of steady state velocities in a curve with and without the cornering rolling resistance force shows that

as corner radius increases, the effect of cornering rolling resistance decreases (Figure 2-16). The cornering rolling resistance has a much lower relative effect at higher velocities as the aerodynamic drag force begins to dominate and the lower lateral accelerations at higher speeds reduce the magnitude of the cornering rolling resistance force. This discrepancy between the cornering effects at lower urban velocities and at highway velocities leads to a logical split of analysis to two sections: highways and urban roads. This split in analysis also supports the differences in road geometry, as highways and urban roads are constructed in drastically different ways. For example, highways utilize banked curves to limit required velocity changes to maintain comfort. Highway curves rarely require velocity decelerations to maintain a maximum lateral acceleration, while urban curves are more involved with larger velocity change events.

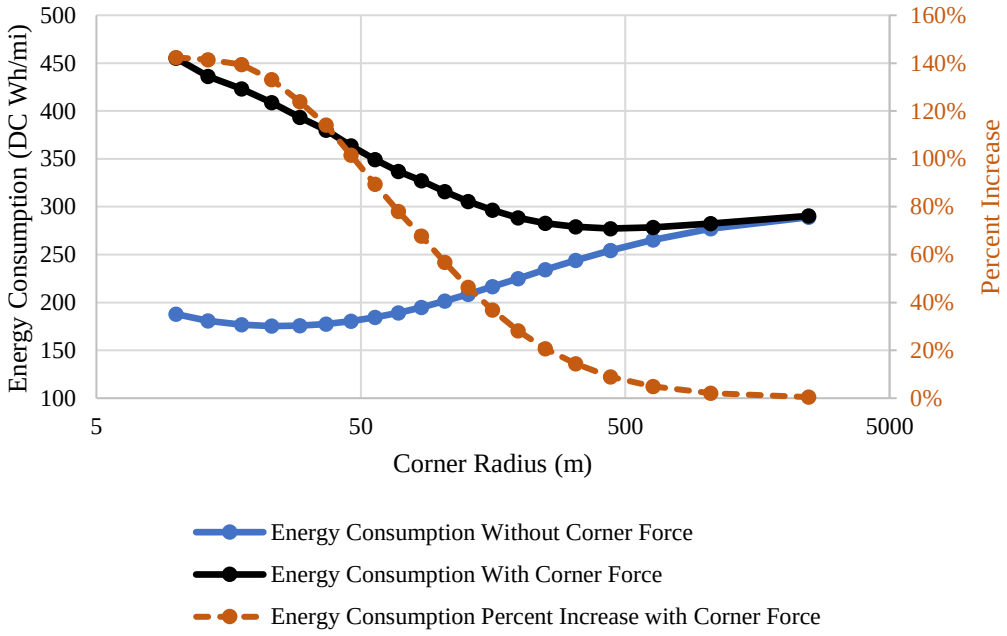

Figure 2-16: Steady state velocity curve comparing the effect on energy consumption when including or excluding the cornering force along a range of common curve radii. Note the logarithmic scale on the x-axis.

2.6.2 Distance Horizons for Usefulness of Curve Inclusion

The significance of the cornering force cannot be ignored at lower urban velocities, but at highway velocities its effect on the total road load force is less than 5% when isolated in a corner. This minimal influence is diminished further when considering the road construction trends of highways compared to urban roads. Highways typically only contain one or two significant curves every few kilometers. The disparity in energy consumption estimates between modeling the corners and not modeling the corners decreases as the overall distance traveled by the vehicle between corners increases. Consumption analysis conducted by iteratively increasing the length of the straight road segment before and after a curve at 90 kph (55 mph) shows the distance horizon at which modeling curves at highway velocities is no longer useful. Figure 2-17 shows when there is greater than 500 meters on either side of a curve, the cornering forces become insignificant across the entire event. Similar analyses conducted at a lower urban velocity of 40 kph (25 mph) show that the distance horizon for urban curves is roughly the same as the highway distance horizon, but the time horizon is much longer – 50 seconds for 40 kph and 30 seconds for 90 kph. The shorter time horizon for urban roads is attributed to the higher lateral accelerations, and in turn cornering rolling resistance force experienced during low speed driving. While the distance horizons are

similar, the likelihood of experiencing a corner less than 500 meters after a previous one is much higher for urban roads when compared to the highway.

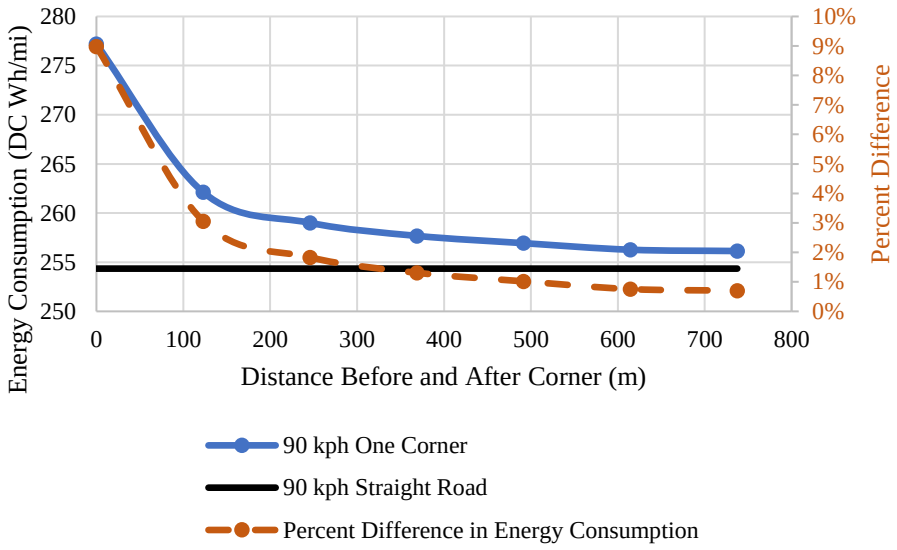

Figure 2-17: Analysis of the distance horizon at which modeling curves at highway speeds (90 kph) is no longer useful.

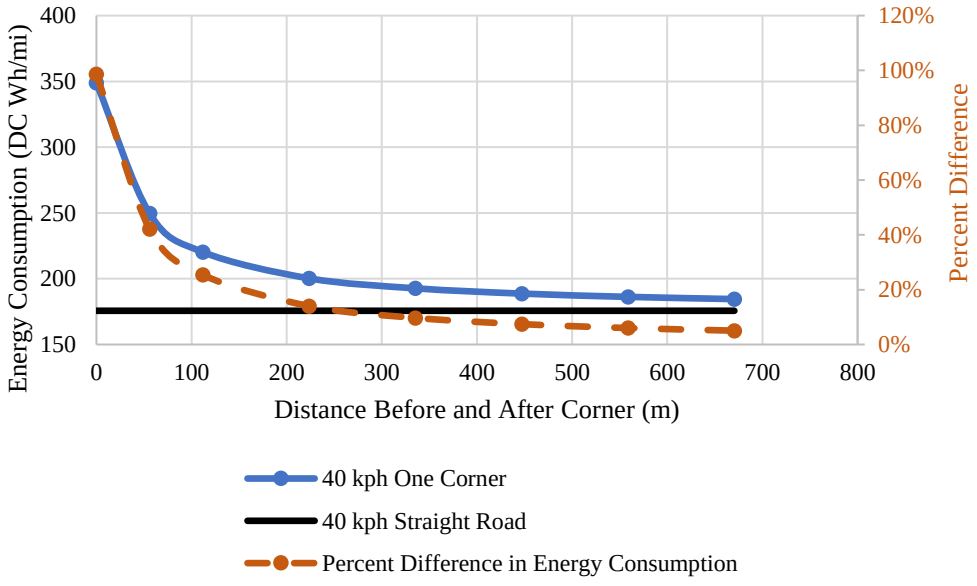

Figure 2-18: Analysis of the distance horizon at which modeling curves at urban speeds (40 kph) is no longer useful.

2.6.3 On-road Results

With the simulation results showing a preliminary conclusion that curves are insignificant during highway travel but important for urban analysis, on-road testing was conducted for more evidence for a 2013 Chevrolet Volt. The on-road route analysis used the same vehicle and test equipment that were used to collect data for the curve transition time and lateral acceleration envelope derivations. The high voltage

(HV) battery pack on the 2013 Chevrolet Volt broadcasts the voltage (V_{batt}) and current draw (I_{batt}) over the vehicle controller area network (CAN) bus. The instantaneous power of the vehicle is calculated with

$$P_{batt} = I_{batt} * V_{batt}, \quad \text{Equation 2-16}$$

and the total event energy is

$$E_{batt} = \int_{t_1}^{t_2} P_{batt} dt. \quad \text{Equation 2-17}$$

2.6.4 Highway and Urban Route Evaluation

On-road full route consumption data is used to test the efficacy of the combined synthesis system of the velocity, curve, and powertrain models. Local routes with frequent curves of known parameters were identified and driven with the instrumented test vehicle to obtain the route energy consumption and velocity trace. The resulting on-road velocity profile was then modeled using the velocity and curve synthesis methods to produce a simulated velocity profile. These simulated profiles are then input into the powertrain model to calculate the estimated energy consumption along the route.

Two unique routes were modeled and validated during on-road testing with the 2013 Chevrolet Volt: a highway route and an urban route. The highway test route is 14.6 km (9.1 miles) long and features three moderate turns with a posted speed limit of 105 kph (65 mph). The corners do not require a vehicle to reduce its speed to comfortably navigate the curve. The urban test route is 1.8 km (1.1 miles) long and features four similar turns that are comparable to most urban right angle corners. Route grade data was generated with manual elevation data entry sampled every 0.1 km. While obtaining reliable road grade data is difficult, studies show that significant grades can decrease vehicle fuel economy up to 20% [2.21]. With no grade data in the analysis, there would be high uncertainty of the true cause of discrepancies between the model results and on-road data.

Figure 2-19 is the time-based urban velocity profile, while Figure 2-20 is the distance-based trace, overlaid with two synthesized velocity traces: one that discredits corners and their associated velocity change events by constantly cruising at the posted speed limit, and one that accounts for road curves. All three routes are distance, not time, constrained. Figure 2-21 is the highway route and its synthesized counterpart. There is only one synthesized highway velocity trace, as the highway curves do not require a change of velocity to maintain comfortable operation. Table 2-2 and Table 2-3 contain the comparisons between the on-road and synthesized profiles for the urban and highway routes, respectively. The tables also compare the value of including or discrediting roadway corners in consumption analysis.

Figure 2-19: Time-based velocity traces for on-road urban route, synthesized mode with velocity changes for corners, and synthesized mode discounting corners (left). Overview of urban route driven to validate corner synthesis and energy consumption techniques with properties of the four corners along the path (right).

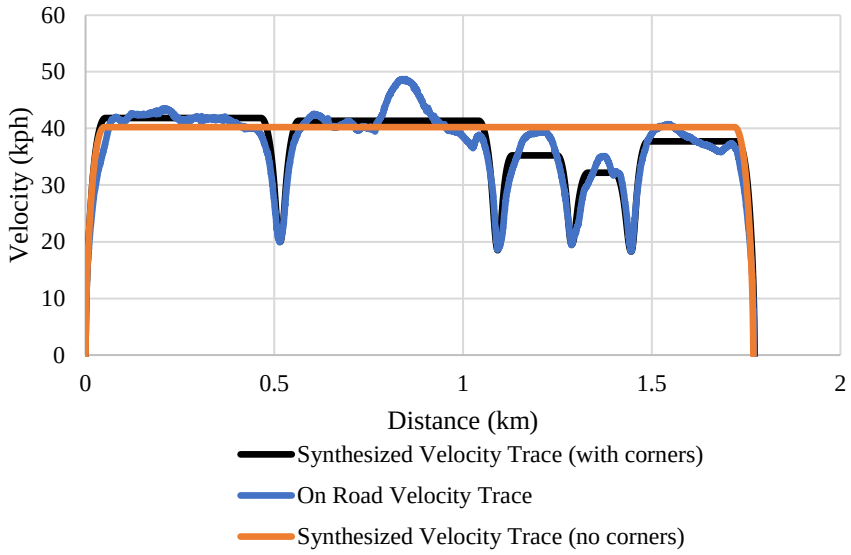

Figure 2-20: Distance-based velocity traces for on-road test, synthesized mode with velocity changes for corners, and synthesized mode discounting corners.

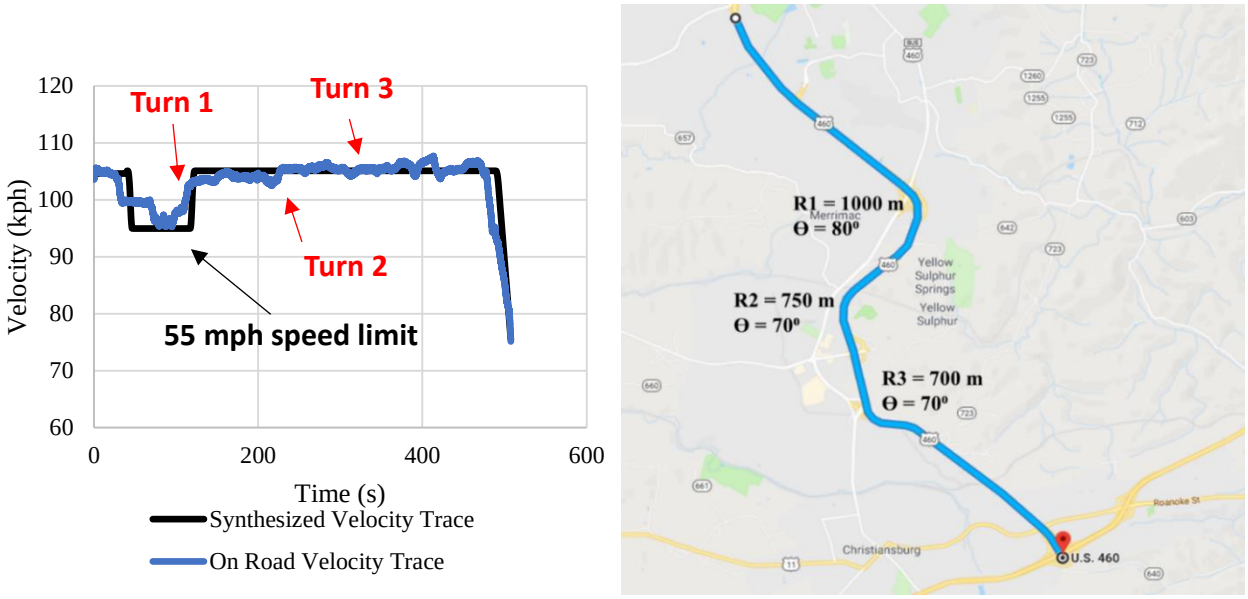

Figure 2-21: Time-based velocity traces for on-road highway route and synthesized velocity mode (left). Overview of highway route driven to validate corner synthesis and energy consumption techniques with properties of the three corners along the path (right).

Table 2-2: Urban Route Synthesis Comparison

Route	**Total Time (s)**	**Average Velocity (kph)**	**Distance (km)**	**Energy Consumption (kJ)**	**Percent Difference from On-road**
Driven On-Road Route	180.7	35.2	1.77	1216.9	-
Synthesized Route (with velocity changes and cornering force)	180.9	35.2	1.77	1196.8	**-1.7%**
Synthesized Route (with only velocity changes)	180.9	35.2	1.77	1147.5	**-5.7%**
Synthesized Route (no curves or velocity changes)	165.9	38.4	1.77	1047.34	**-14.9%**

Table 2-3: Highway Route Synthesis Comparison

Route	Total Time (s)	Average Velocity (kph)	Distance (km)	Energy Consumption (kJ)	Percent Difference from On-road
Driven On-Road Route	507.7	103.1	14.53	9433.5	-
Synthesized Route (with curves)	507.7	103.1	14.53	9433.6	**0.1%**
Synthesized Route (no curves)	507.7	103.1	14.53	9416.8	**-0.1%**

The urban route comparison results show the most accurate synthesis method is the mode that included both the velocity change events and the cornering force. The 1.7% error between synthesized mode and on-road consumption data shows that including cornering effects in urban route modeling does increase model fidelity. The velocity trace shows that the test driver did not drive the corners as modeled, as the driver was not instructed to drive the curves in any specific way. The result is that the velocity profiles of the driven curves are shaped differently than the synthesized curve used for modeling. The driver began entering the curve before they fully decelerated to the cornering velocity. An analysis indicates that the resulting energy consumption of the naturalistic on-road corner and the synthesized corner is different by only 3%. The on-road supplemental appendix contains more detail on the corner specific comparison. Another factor to consider when including cornering is the travel time penalty associated with navigating these curves at lower velocities. When strictly considering energy consumption modeling, time is not a primary concern. However, it will be important to note travel time penalties accrued from curves for eco-routing purposes, as the overall travel time on the road influences a driver's decision when choosing between using an eco-route or not.

The error between the synthesized and on-road results for the highway route is much lower than the urban route, regardless of whether or not cornering forces are included. This is attributed to the consistently high magnitude of the aerodynamic drag force at highway speeds when compared to grade, tire rolling resistance, or inertial forces. The aerodynamic force is straightforward to model, as longitudinal velocity traces are trivial to synthesize, and results in a low model uncertainty. The lack of required velocity changes to comfortably navigate a curve at highway speeds eliminates the influence of inertial forces on consumption.

2.7 Conclusion and Future Work

Vehicle simulations and on-road testing suggest road corners have a negative effect on vehicle energy consumption. The magnitude of the influence of cornering is dependent on the vehicle velocity, and road type and geometry. The consumption error between a synthesized urban route and its on-road counterpart decreased from a 14.9% energy consumption error, when excluding corners, to a 1.7% energy consumption error when including curves. The influence of cornering is greater at lower velocities due to humanistic tendencies for higher lateral accelerations in urban environments and the prevalence of more involved road corners at lower velocities. The higher curvature corners also require significant vehicle velocity changes for safe and comfortable curve navigation, which adds travel time and energy use penalties when compared to straight road driving. The vehicle deceleration and acceleration effects are magnified or diminished depending on the powertrain of the tested vehicle. A BEV utilizes regenerative braking which recaptures a large portion of the energy lost during deceleration, while an ICEV loses all of that energy in the form of heat. Using an ICEV in the above analysis would increase the disparity between the no-corner energy consumption modeling method and the on-road results.

At higher speeds and on less corner-dense highways, the effect of cornering on overall route energy consumption is much lower. Drivers prefer to maintain lower lateral acceleration levels, when compared with urban lateral acceleration levels, at highway velocities. This lower lateral acceleration correlates to a smaller corner rolling resistance force that is already negligible when compared to the aerodynamic drag force at highway speeds. Coupling this relatively small force with the low frequency of curves on highways results in a < 1% fluctuation in energy consumption estimations when including or excluding corners in analysis.

Incorporating this work into an integrated eco-routing system will increase the fidelity of predetermining route energy consumption and ensure the most energy efficient route is chosen. The lateral acceleration envelope and longitudinal acceleration limits can be calibrated for a driver, through obtaining lateral acceleration versus velocity data over a preliminary calibration period, to generate an individual profile that further matches real-world expected route energy consumption. Replacing the human behavior generalizations made above will further increase the accuracy of energy use modeling. In addition to improved modeling accuracy, this work opens the door to vehicle corner navigation optimization for reducing fuel use. Decreasing lateral acceleration will reduce the corner rolling resistance but increase the time penalty of the turn due to the lower cornering velocity. Another optimization opportunity presents itself in BEV and PHEV regenerative braking control. Planning longitudinal deceleration events where the maximum deceleration value is paired with the maximum regenerative braking deceleration will ensure maximum energy recapture while limiting frictional braking usage. More analysis over a wider range of urban or rural routes will give a better picture of when to include or exclude corners in energy consumption analysis.

2.8 References

[2.1] Ahn, K. and Rakha, H., "Network-wide impacts of eco-routing strategies: A large-scale case study," Transportation Research D, vol. 25, pp. 119-130, Dec. 2013.

[2.2] Richter, M., Zinser, S., and Kabza, H., "Comparison of Eco and Time Efficient Routing of ICEVs, BEVs and PHEVs in Inner City Traffic," Vehicle Power and Propulsion Conference (VPPC), 2012 IEEE, Seoul, 2012, 1165-1169.

[2.3] Ericsson, E., Larsson, H., and Brundell-Freij, K., "Optimizing Route Choice for Lowest Fuel Consumption- Potential Effects of a New Driver Support Tool," Transportation Research Part C: Emerging Technologies 14(6):369-383, 2006.

[2.4] Moniot, M. and Nelson, D., "Synthesis of speed versus time modes using variable acceleration rates for tractive energy analysis and route planning", to be submitted for publication.

[2.5] Warpe, H., Moniot, M., Nelson, D., and Baumann, W., "EcoRouting Strategy Using Variable Acceleration Rate Synthesis Methodology," SAE Technical Paper 2018-01-5005, 2018, doi:10.4271/2018-01-5005.

[2.6] Bigazzi, A., Clifton, K., and Gregor, B., "Modeling the Effects of Congestion on Fuel Economy for Advanced Powertrain Vehicles," Transportation Research Board 91st Annual Meeting, Jan. 2012.

[2.7] Holden, J. et al., "Development of a Trip Energy Estimation Model using Real-World Global Positioning System Driving Data," National Renewable Energy Laboratory, ITS World Congress, Montreal, CA, Oct. 2017.

[2.8] AASHTO. AASHTO Green Book: A Policy on Geometric Design of Highways and Streets. American Association of State Highway and Transportation Officials, 444 North Capitol Street, N.W., Suite 249, Washington, D.C. 20001, 5th edition, 2004.

[2.9] Ai, C. and Tsai, Y., "Automatic Horizontal Curve Identification and Measurement Method Using GPS Data," Journal of Transportation Engineering, vol. 141, Issue 2, Feb. 2015.

[2.10] Theodosis P. and Gerdes, J., "Generating a Racing Line for an Autonomous Racecar Using Professional Driving Techniques," ASME 2011 Dynamic Systems and Control Conference, Arlington, VA, Oct. 2011.

[2.11] Meidenbauer, K., "An Investigation of the Clothoid Steering Model for Autonomous Vehicles," M.S. Thesis, Dept. Mech. Eng., Virginia Tech, Blacksburg, VA, 2007.

[2.12] Kritayakirana, K., "Autonomous Vehicle Control at the Limits of Handling," Ph. D Dissertation, Dept. Mech. Eng., Stanford University, Stanford, CA, 2012.

[2.13] Eager, D., Pendrill, A., and Reistad, N., "Beyond velocity and acceleration: jerk, snap, and higher derivatives," European Journal of Physics, vol. 37, no. 6, Oct. 2016.

[2.14] Odhams, A. and Cole, D., "Models of Driver Speed Choice in Curves," 7th International Symposium on Advanced Vehicle Control, pp. 439-444, Arnheim, the Netherlands, Aug. 2004.

[2.15] Reymond, G. et al., “Role of Lateral Acceleration in Curve Driving: Driver Model and Experiments on a Real Vehicle and a Driving Simulator,” The Journal of Human Factors and Ergonomics Society, vol. 43, issue 3, pp. 483-495, Sept. 2001.

[2.16] Hugemann, W., “Longitudinal and Lateral Accelerations in Normal Day Driving,” 6th ITAI International Conference, Stratford-upon-Avon, UK, 2003.

[2.17] Tamaro, C., "Vehicle powertrain model to predict energy consumption for ecorouting purposes," M.S. Thesis, Dept. Mech. Eng., Virginia Tech, Blacksburg, VA, 2016.

[2.18] White, E., Nelson, D., and Manning, C., “An Illustrative Look at Energy Flow through Hybrid Powertrains for Design and Analysis,” SAE Technical Paper, 14. http://doi.org/10.4271/2015-01-1231, 2015

[2.19] Argonne National Laboratory, *Downloadable Dynamometer Database*, 2018, Available: https://www.anl.gov/energy-systems/group/downloadable-dynamometer-database

[2.20] Rahman, K., Anwar, M., Schulz, S., Kaiser, E. et al., "The Voltec 4ET50 Electric Drive System," SAE World Congress, https://doi.org/10.4271/2011-01-0355, Jan. 2011.

[2.21] Boriboonsomsin, K., and Barth, M., “Impacts of Road Grade on Fuel Consumption and Carbon Dioxide Emissions Evidenced by Use of Advanced Navigation Systems,” Transportation Research Record. 2139, pp. 21-30. 10.3141/2139-03, 2009.

3 Supplemental Appendices

The following appendices contain additional information and more detailed explanations of concepts brought forth in the preceding journal paper.

3.1 Investigation of Resistive Force Experienced in a Corner

The road load forces experienced by a vehicle are the driving metrics for estimating energy use along a route. The forces experienced by a vehicle, not including grade force, on a road are defined by either a set of two or three terms. The two term method consists of two force terms: a constant velocity-independent rolling resistance term and a velocity influenced aerodynamic drag force. These two variables are defined as,

$F_{aero} = \frac{1}{2}\rho_{air} C_d A_f v^2$ and Equation 3-1

$F_{RR} = mgC_{rr}$. Equation 3-2

Where,

ρ_{air} = density of air,

C_d = coefficient of aerodynamic drag of vehicle,

A_f = frontal area of vehicle,

v = velocity of vehicle,

m = test mass of vehicle,

g = acceleration due to gravity in m/s^2, and

C_{rr} = coefficient of rolling resistance.

The resulting vehicle road load force is

$F_{RL} = F_{RR} + F_{Aero}$. Equation 3-3

The second method for quantifying vehicle road load forces is a three-term equation that is experimentally calibrated to match real-world vehicle test data. The road load equation in its general form as a function of vehicle velocity is

$F_{RL} = A + Bv + Cv^2$. Equation 3-4

The ABC coefficients are vehicle specific and are found empirically through an analysis of vehicle coastdown tests. They can also be associated to physical vehicle specific properties, as this allows the ABC values to be scaled appropriately with changing minor vehicle properties (i.e. mass, frontal area, and tire properties). A is the velocity-independent force due to tire rolling resistance, B is the velocity-dependent force that includes the drivetrain loss and additional rolling resistance, and C is the vehicle aerodynamic drag. Equations 3-5, 3-6, and 3-7 show the physical property equivalents of the ABC coefficients. Note that C_{rr0} or C_{rr1} are not the same as C_{rr} from equation 3-2.

$A = mgC_{rr0}$ Equation 3-5

$B = mgC_{rr1}$ Equation 3-6

$$C = \frac{1}{2}\rho_{air} C_d A_f$$ Equation 3-7

This cornering force analysis uses the three-term method, as the vehicle powertrain model also uses this method for its energy consumption estimates. Table 3-1 contains the test vehicle parameters used in the cornering force analysis. These values correspond to a 2013 Chevrolet Volt, the vehicle used for on-road testing. The road load coefficients and driveline characteristics are from the Argonne National Lab Downloadable Dynamometer Database [3.1]. The vehicle cornering stiffness is a function of individual tire load and wheel size [3.2].

Table 3-1: Vehicle parameters used during cornering force derivation and analysis.

Name	Variable	Value	Unit
Test Mass	m	1,814	kg
Cornering Stiffness	C_α	63,000	N/rad
Road load A coefficient	A	116.6	N
Road load B coefficient	B	2.87	N/(m/s)
Road load C coefficient	C	0.330	N/(m/s^2)
Constant rolling resistance coefficient	C_{RR0}	0.00655	-
Velocity-dependent rolling resistance coefficient	C_{RR1}	0.000161	1/(m/s)
Vehicle frontal area x coefficient of drag	$A_{F*}\, C_d$	0.55	m^2
Density of air	ρ_{air}	1.2	kg/m^3

The bicycle model is commonly used to analyze lateral forces acting on a vehicle at higher speeds [3.3]. The bicycle model reduces the individual properties of the two front and rear tires into a single pair of front and rear wheels. The bicycle model assumes negligible lateral roll and lateral weight shift. These assumptions, however, are not valid under speeds of 15 mph because of the prevalence of Ackermann steering at lower velocities. Ackermann steering geometry turns the front wheels at slightly different angles to account for the axle width of a vehicle during a turn to ensure both the left and right turning wheels follow an equal curve radius. Ackermann steering reduces tire scrubbing and wear. At higher velocities the steering angles are much less compared to the angles at lower speeds, thus Ackermann steering effects are considered negligible [3.4].

Figure 3-1 is the free body diagram of the bicycle model where α_f is front tire slip angle, α_r is rear tire slip angle, F_{LatF} is the lateral force on the front tire, F_{LatR} is the lateral force on the rear tire, F_C is the centripetal force, and δ is the vehicle steering angle. The tire slip angles occur when the vehicle is turning because of tire deformation under loading from the front and rear lateral forces. The slip angle response to lateral force increases linearly until the upper frictional limits of the tire are met, typically up to 8º. After this, the response to lateral force is non-linear. This non-linear region is not experienced during normal passenger tire use [3.2]. When a tire slip angle develops, a tire rolling resistance manifests because the tire direction of travel is not orthogonal to the lateral tire force. The detailed free body diagram of the front wheel in figure 3-2 shows this effect.

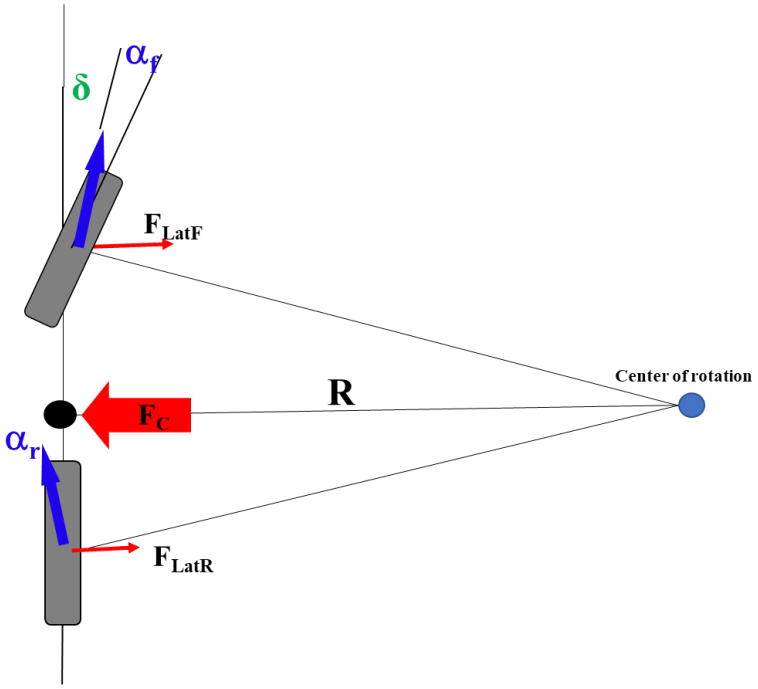

Figure 3-1: Bicycle model free body diagram of a vehicle executing a right-hand turn.

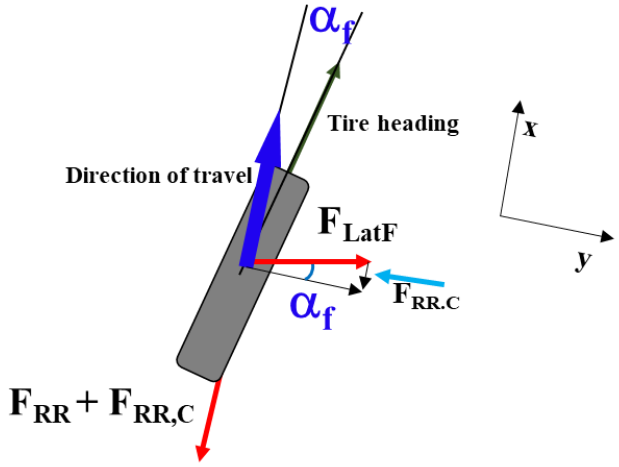

Figure 3-2: Free body diagram of the front tire of a bicycle model during a cornering event. The direction of travel and $F_{RR,C}$ are parallel. From [3.5].

The cornering rolling resistance force is a function of cornering stiffness and tire slip angle.

$$F_{RR,CF} = F_{LatF}\sin(\alpha_F) \approx C_{\alpha F}{\alpha_F}^2 \quad \text{Equation 3-8}$$

$$F_{RR,CR} = F_{LatR}\sin(\alpha_R) \approx C_{\alpha R}{\alpha_R}^2 \quad \text{Equation 3-9}$$

Where:

$$F_{Lat} = C_\alpha \alpha \quad \text{Equation 3-10}$$

$$\sin(\alpha) \approx \alpha$$ Equation 3-11

The small angle approximation of the sine term is acceptable, as the slip angle is no greater than 8º during normal operation. The cornering stiffness, C_α, of a vehicle is a dynamic metric that describes the lateral compliance present in the system. The vehicle used in this analysis is assumed to have equal slip angles between the front and rear tires,

$$\alpha_f = \alpha_r$$ Equation 3-12

This is also known as neutral steer and occurs when a vehicle has an exact 50/50 front to rear weight distribution [3.3]. Although the 2013 Chevrolet Volt does not have a 50/50 weight distribution, this assumption simplifies the analysis and eliminates the need for weight distribution modeling of the vehicle during a route. Modeling dynamic vehicle weight distribution is beyond the scope of this research.

The resistive force due to cornering is a result of a constant vehicle cornering stiffness and a changing slip angle that is a result of how a corner is driven. Relating slip angle to lateral acceleration will further limit the required analysis at each corner, as the maximum lateral acceleration envelope in Figure 2-12 can be used to predict slip angle before the cornering event. Further defining slip angle gives

$$\alpha = \frac{mv^2k}{C_\alpha},$$ Equation 3-13

where v^2k is the lateral acceleration and m is the test mass of the vehicle. Substituting Equation 3-13 into Equation 3-8 and 3-9 yields

$$F_{RR,C} = \frac{m^2a_{lat}^2}{2C_\alpha}.$$ Equation 3-14

This relationship between lateral acceleration and rolling resistance force due to cornering shows that the force is independent of vehicle velocity and instead based on driver cornering behavior. The maximum cornering rolling resistance at any curve velocity is found by using the lateral acceleration envelope in Figure 2-12. An analysis using 2013 Chevrolet Volt road load properties shows the expected cornering rolling resistance force for a range of lateral accelerations in Figure 3-3. Comparing the cornering force effect with the expected lateral accelerations at certain cornering velocities shows the influence is small at highway speeds with lower lateral accelerations. The cornering effect is much greater during lower velocity corners between speeds of 15 to 60 kph where the lateral acceleration is greater. This initially indicates a larger energy impact of corners on urban and low speed rural routes as opposed to high velocity highway routes.

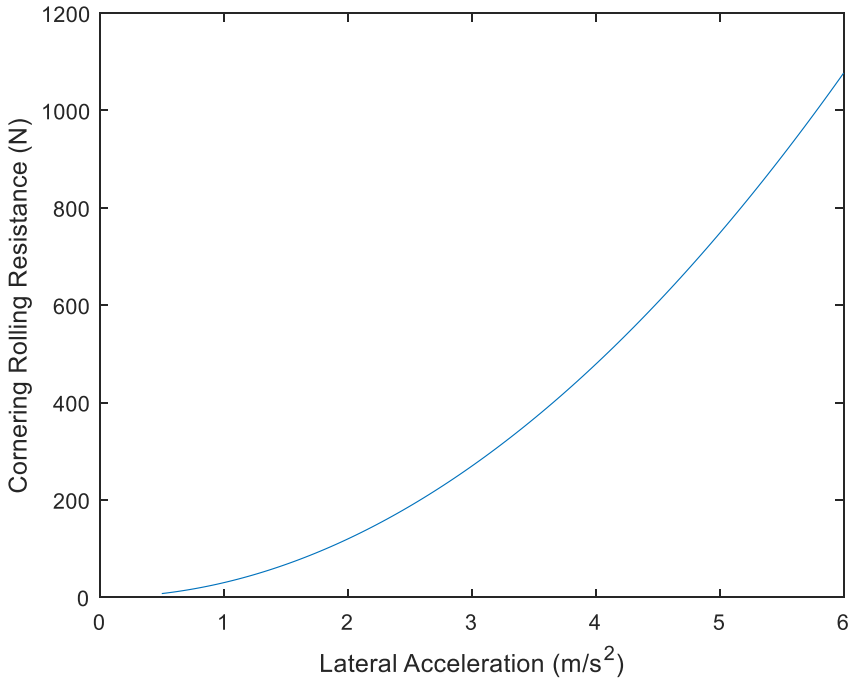

Figure 3-3: Cornering rolling resistance force for a range of lateral accelerations using 2013 Chevrolet Volt properties from Table 3-1.

One of the main goals of this research is to simplify the modeling process by limiting the number of required inputs to an energy consumption model. Adding the turning rolling resistance term increases the model fidelity but it also increases the complexity. Cornering stiffness is not a commonly available vehicle parameter. As mentioned above, the value used for the 2013 Chevrolet Volt is an approximation derived from empirical data in [3.2]. An analysis with a wide range of cornering stiffness values shows the effect of changing cornering stiffness on the cornering rolling resistance force. The cornering stiffness input varies between 35,000 and 100,000 N/rad to ensure that a wide breadth of passenger vehicles are included in the analysis. The maximum lateral acceleration value is set as 2.5 m/s^2. Figure 3-4 is a plot of the effect cornering stiffness has on the cornering rolling resistance force. The cornering stiffness a function of how compliant the vehicle suspension and tires are around a curve. A more compliant system increases the force of cornering rolling resistance on the vehicle.

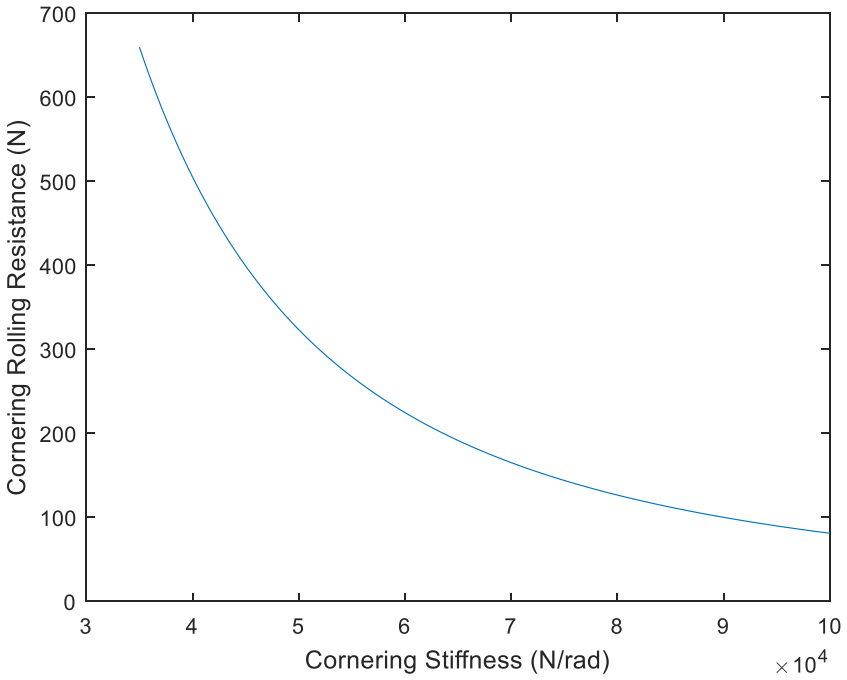

Figure 3-4: The effect of vehicle cornering stiffness on the cornering rolling resistance force with a set lateral acceleration of 2.5 m/s^2.

3.2 2013 Chevrolet Volt Powertrain Model

The powertrain model used in this thesis is a backward-facing model developed by [3.6] and [3.7]. The model is constructed so that it can be tuned and validated using publicly available data from chassis dynamometer energy consumption testing [3.1]. [3.1] has dynamometer results for common drive cycles, steady state velocity tests, and coastdown tests.

Two common methods to model vehicle power requirements along a time and velocity route are the backward-facing or forward-facing models. Forward-facing models are composed of a simulated vehicle powertrain model that responds to a velocity demand as an input. The output of the model is the resulting vehicle velocity trace once the velocity request works through the vehicle control systems. The modeled vehicle powertrain includes the logic for defining required power to achieve the desired velocity, and the resulting velocity is calculated by simulating the power flow through the engine or motor, transmission, and then drive wheels. As the vehicle velocity request is the input, the required power flow includes delays in engine torque output, driveline inertia, and wheel slip. Forward-facing models also incorporate powertrain limitations such as vehicle top speed or maximum acceleration, which permit the possibility of velocity trace misses. These modeled physical limitations usually cause a delay, or error, between the requested velocity traces and the resulting vehicle model velocity. This error between requested and resulting velocities reduce the ability of the forward-facing model to calculate the energy consumption along a route. Forward-facing models are most useful for the development of realistic control strategies (i.e. shifting, traction control), as they more closely resemble natural operation of a vehicle.

The backwards-facing model is the accepted method in which the energy consumption along a route is calculated. In contrast to the forward-facing model, a backwards-facing model uses the desired route, velocity and time trace, as the input. The simulation input flows backwards through the powertrain model and determines the power and torque needed to satisfy the desired velocity at the wheels. There are, however, some limitations of this modeling technique. One of which is that the maximum speed or power of the powertrain cannot be enforced. This model disadvantage is overlooked for this energy consumption model, as all modern vehicles have the necessary power to adhere to common roadway speed limit and acceleration requirements.

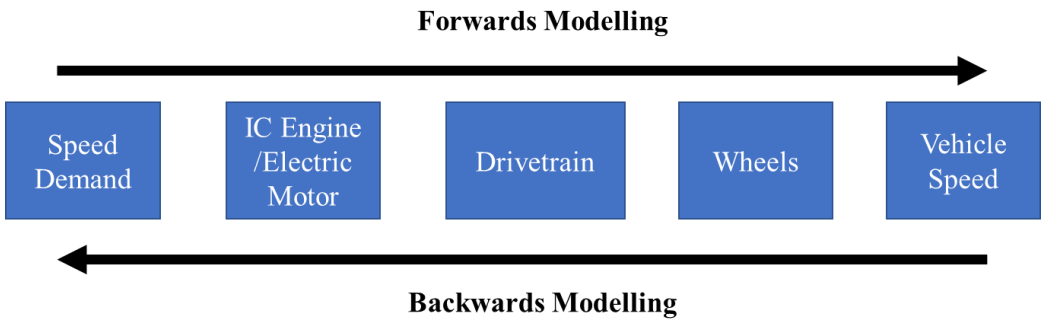

Figure 3-5: Differences in the approaches of forwards and backwards facing vehicle modeling techniques from [3.8].

As mentioned, the powertrain model is tuned and validated with dynamometer test data. A common drive cycle for model validation is the steady state speed step drive cycle. This schedule consists of starting at 0

mph and stepping velocity up by 10 mph roughly every 20 seconds to 80 mph and then back down to 0 mph. The 0-80-0 steady state schedule is useful, as it isolates a range of velocities and acceleration events so that it is clear where the model and dynamometer results diverge. Figure 3-6 is the 0-80-0 steady state velocity trace with the battery SOC results from the powertrain model and the dynamometer results. Figure 3-7 is the same 0-80-0 steady state velocity trace but instead overlaid with the SOC error between the dynamometer and model. This shows at what conditions the two results deviate. Acceleration and deceleration events at velocities above 65 mph are the main cause of error between the powertrain model and dynamometer test results. This is an acceptable error, as the speed limit on the driven highway route was either 55 mph or 65 mph.

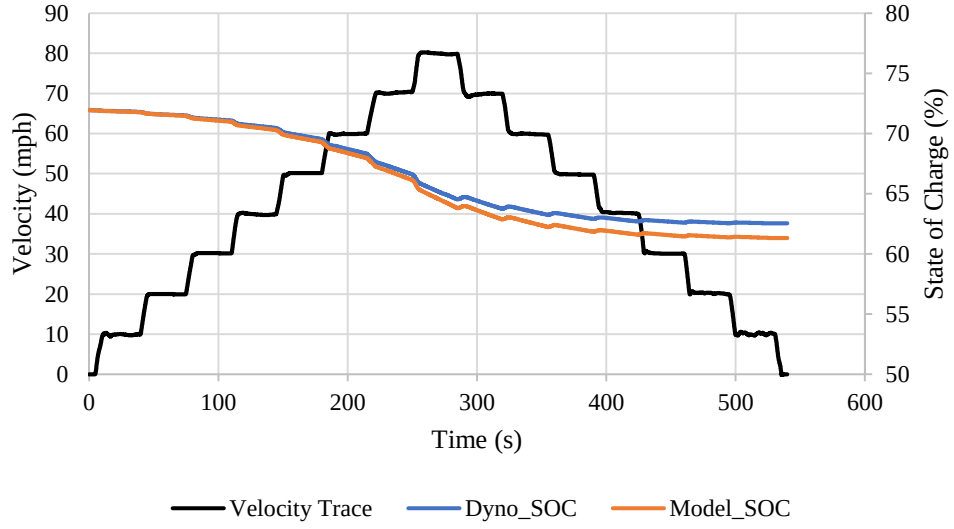

Figure 3-6: Modeled Volt SOC compared against dynamometer Volt SOC for 0-80-0 mph steady state speed step cycle.

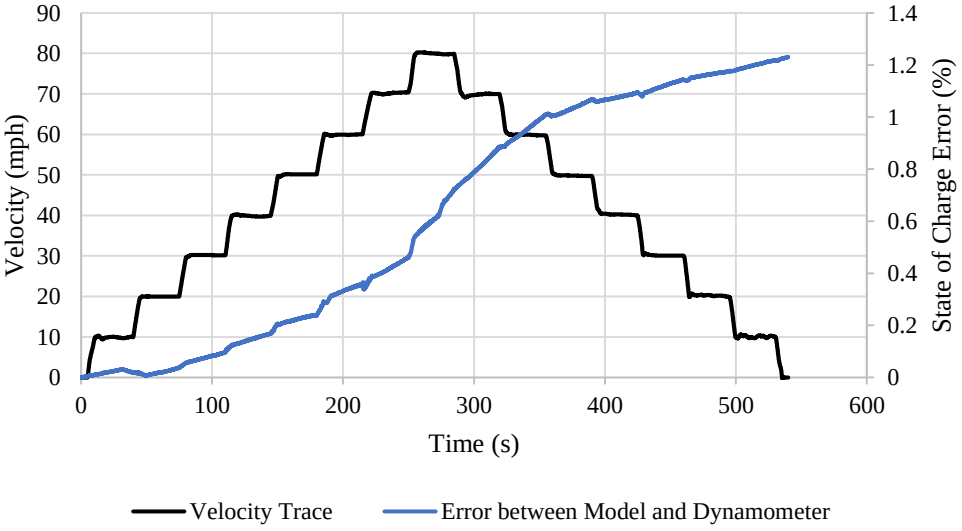

Figure 3-7: SOC error between vehicle modeled 0-80-0 SS drive cycle and dynamometer results. The error increases more quickly at higher velocities indicating there are slight discrepancies at higher velocities between the model and dynamometer results.

The powertrain and vehicle characteristics in Table 3-2, 3-3, and 3-4 are for a 2013 Chevrolet Volt. They were obtained from either the dynamometer test database or from the baseline vehicle parameters in [3.9].

Table 3-2: Powertrain model vehicle glider characteristics

Vehicle Glider Characteristics		
Parameter	Value	Units
C_{rr0}	0.00655	[---]
C_{rr1}	0.000161	[1/(m/s)]
C_d	0.231	[---]
A	2.38	[m^2]
C_dA	0.55	[m^2]
ρ_{air}	1.2	[kg/m^3]
Cornering Stiffness	63000	[N/rad]
m	1814	[kg]
m_i factor	1.04	[---]
m_i	1887	[kg]
g	9.81	[m/s^2]
r_w	0.355	[m]
P_{acc}	750	[W]

Table 3-3: Powertrain model regenerative braking and driveline characteristics

Regen Characteristics			Driveline Characteristics		
Parameter	Value	Units	Parameter	Value	Units
Regen Fraction	0.88	[---]	Gear Ratio	7.8	[---]
Regen V_{min}	2	[m/s]	N/V	210	[rpm/mps]
Regen $-P_{tr,lim}$	-45	[kW]	N/V	93.8	[rpm/mph]
Regen $-T_{w,lim}$	-770	[Nm]	Top Speed	101	[mph]
Regen $-F_{tr,lim}$	-2.17	[kN]			

Table 3-4: Powertrain model motor and battery characteristics

Motor Characteristics			Battery Characteristics		
Parameter	Value	Units	Parameter	Value	Units
$k_c*T_{ref}^2$	7000	[W]	V_{oc}	355	[V]
$k_i*\omega_{ref}$	700	[W]	R_{int}	0.150	[ohm]
$k_w*\omega_{fef}^3$	450	[W]	E_{cap}	16500	[Wh]
C	275	[---]	m_{batt}	197	[kg]
k_p	0.0	[---]	$SOC_{initial}$	71.9	[%]
T_{max}	370	[Nm]	Δ SOC	88	[%]
T_{loss}	1.5	[Nm]	CS SOC Target	30	[%]
T_{ref}	370	[Nm]	CS SOC Window	10	[%]
ωbase	500	[rad/s]	$\eta_{charger}$	90	[%]
$\omega_{ref,base}$	300	[rad/s]			
$T_{ref}*\omega_{ref}$	111000	[Nm*rad/s]			
S_{base}	2850	[rpm]			
S_{max}	9500	[rpm]			
Pmot	110.4	[kW]			
Mot Eff =	92.9%	Tmax*Sbase			

3.3 Details of On-road Testing

On-road testing is used to derive the naturalistic cornering easement times, validate the lateral acceleration and velocity envelope, and validate the synthesized corner energy consumption model. The vehicle used for testing is a stock 2013 Chevrolet Volt plug-in hybrid vehicle. The Volt travels an EPA-labeled 38 miles on electricity from the battery pack before the internal combustion engine turns on. The simplicity of modeling a BEV compared to an ICEV resulted in only testing the vehicle during its all-electric operating range.

Data is collected using a Raspberry Pi and CAN analysis tools. The Pi is outfitted with a Sense Hat with 3-axis accelerometers and 3-axis angular rate sensors. These sensors enable acquisition of the cornering rate and in-turn lateral acceleration. The Pi interfaces with MATLAB on a laptop computer for data acquisition and analysis. Vehicle velocity, HV battery voltage, and HV battery current is acquired by tapping into the vehicle CAN network through the OBDII port. Reading the CAN values into MATLAB enables matching vehicle velocity, HV battery current, and HV battery voltage to the accelerometer and angular rate data at an acquisition rate of 25 Hz.

The two tested routes are driven as the energy out of the battery is monitored and matched with the vehicle speed. The journal paper section of this thesis contains the velocity traces of the two routes. Road grade data is manually found post-test by determining elevation at various points along the route and, in turn, grade percentage is calculated from the rate of change of the elevation. Figures 3-8 to 3-11 are the resulting power demand and energy demand for the highway and urban routes.

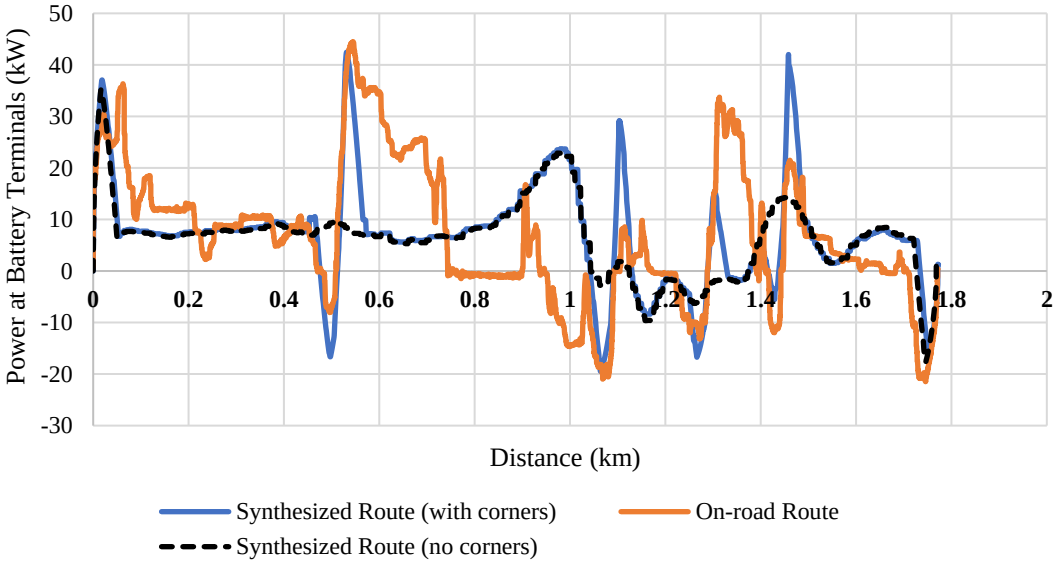

Figure 3-8: Distance-based power at the battery terminals for the driven and synthesized urban route.

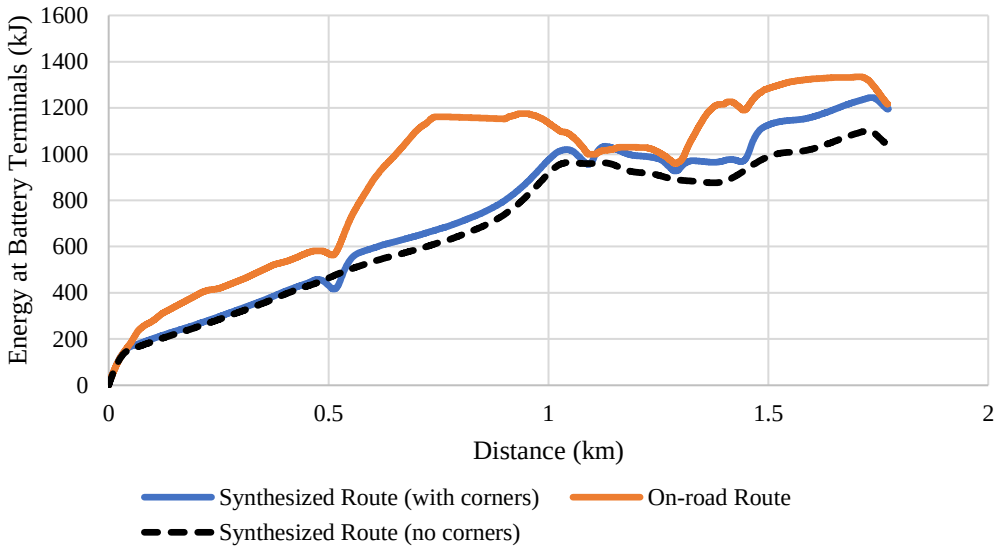

Figure 3-9: Distance-based energy consumption results for the driven and synthesized urban route.

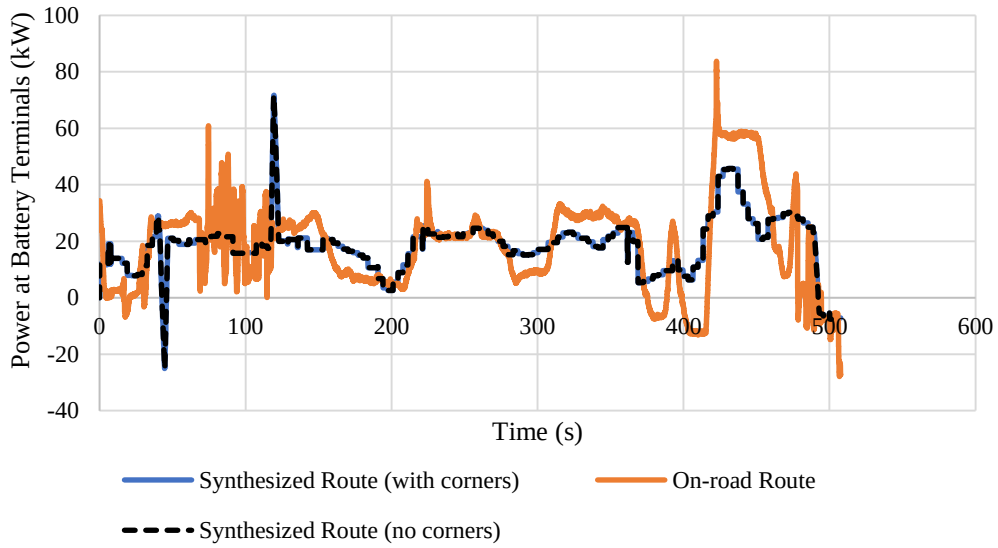

Figure 3-10: Distance-based power at the battery terminals for the driven and synthesized highway route.

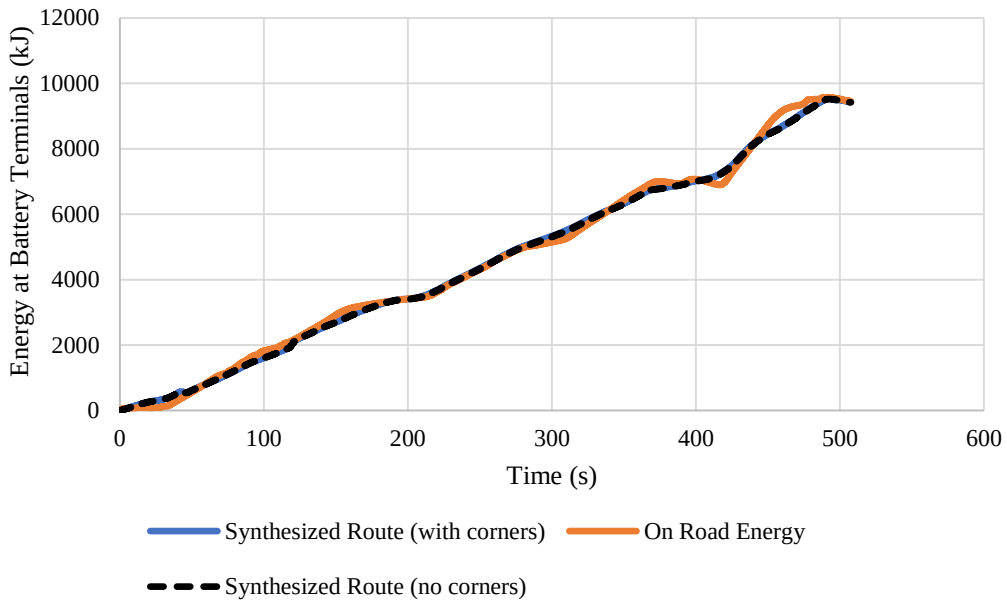

Figure 3-11: Time-based energy consumption results for the driven and synthesized highway route.

One concern of this analysis is how to direct the test driver to navigate a curve during route testing. As discussed in the journal paper, the model assumes the driver fully decelerates to cornering velocity before entering the curve. This eliminates the snap, the 4th derivative of position, experienced by the vehicle passengers; however, this is not indicative of how the average driver typically navigates a curve. The test driver was instructed to drive a corner as they usually would during preliminary testing. Analysis shows the differences between the modeled and actual driven corner. Figure 3-12 shows that while the two velocity traces are shaped differently, the time to complete the event is roughly the same. The average velocities of the on-road and synthesized curves are 9.1 m/s and 8.4 m/s, respectively. The energy consumptions of the on-road and synthesized curves are 280.6 DC Wh/mi and 272.6 DC Wh/mi, respectively. This corresponds to a consumption error of 3% between the modeled and driven curve. Over the course of an entire drive cycle, this small error does not have a significant effect on the overall consumption results.

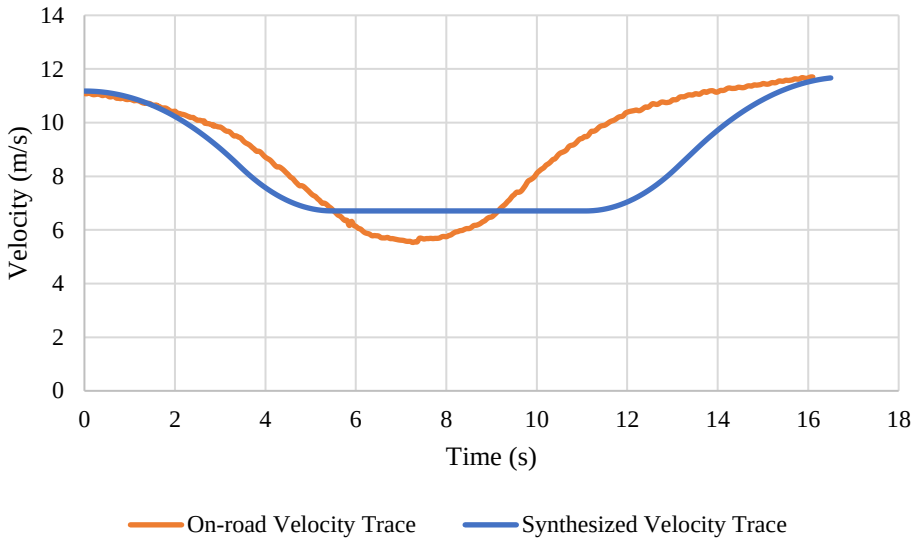

Figure 3-12: Comparison of velocity traces from the modeled curve and the on-road driven curve.

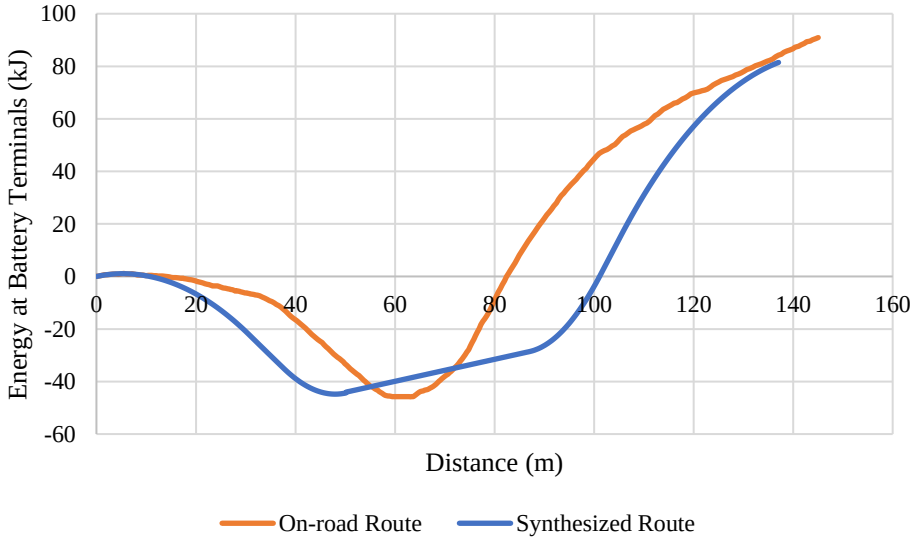

Figure 3-13: Comparison of energy consumption of the modeled curve and the on-road driven curve.

3.4 Eco-routing Curve Penalty Look-up Table

Another method for incorporating curves into energy consumption analysis, or eco-routing, is implementation of a curve penalty look-up table. Analyzing a wide range of curve shapes and building a general reference table that includes the energy consumption and travel time penalties of most common roadway curves will decrease the required computation for estimating energy consumption and travel time along a curving route. This brief analysis is a proof of concept for a curve penalty reference table. A route is first modeled with no curves. Then, similar curves are iteratively added to the route to determine the total energy use and travel time increase.

To evaluate the effect of increasing the number of turns on a route, a baseline straight-road velocity profile is first generated using the hill model defined in the journal paper section of this thesis. This profile has a cruise velocity of 35 mph and a total travel distance of 0.68 miles. The distance is constrained to 0.68 miles for each analyzed route to ensure consistent energy comparisons across all cases. The energy consumption along this baseline route found using a 2013 Chevrolet Volt powertrain model is 226.3 DC Wh/mi.

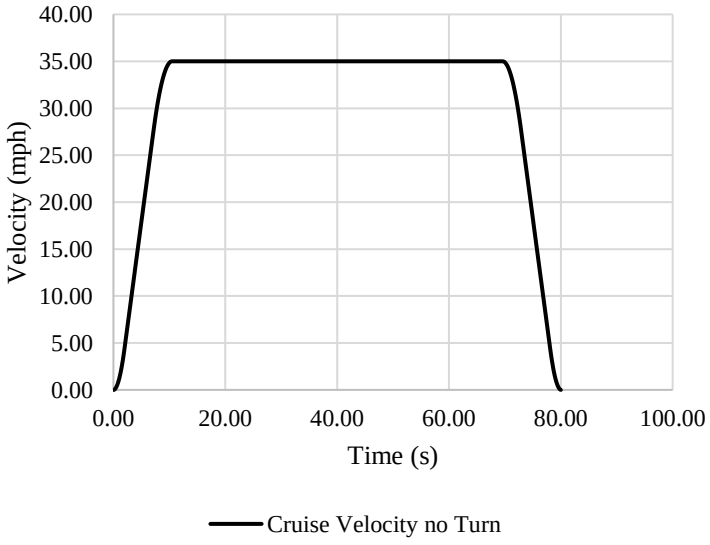

Figure 3-14: Velocity profile as a function of time for a no-turn synthesized route.

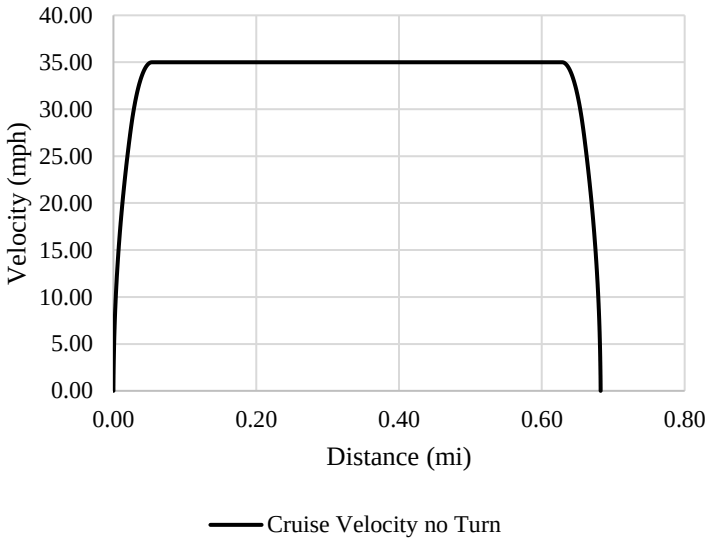

Figure 3-15: Velocity profile as a function of distance for a no-turn synthesized route.

Next, turns are added to the velocity mode iteratively while the distance and cruise velocities of the modes are constrained. Constraining the distance of the modes isolates the curve energy consumption effects. The time was not constrained to evaluate the time penalties associated with adding turns to a route. The plots below show the cruise velocity mode compared with one, two, and three turn velocity modes. Each added turn is a 90-degree curve with a 15 meter radius taken at 15 mph.

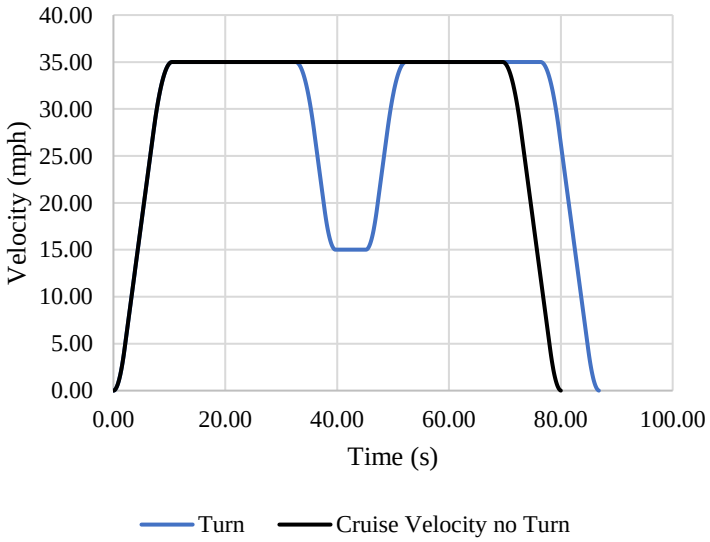

Figure 3-16: Velocity profile as a function of time for a two-turn synthesized route.

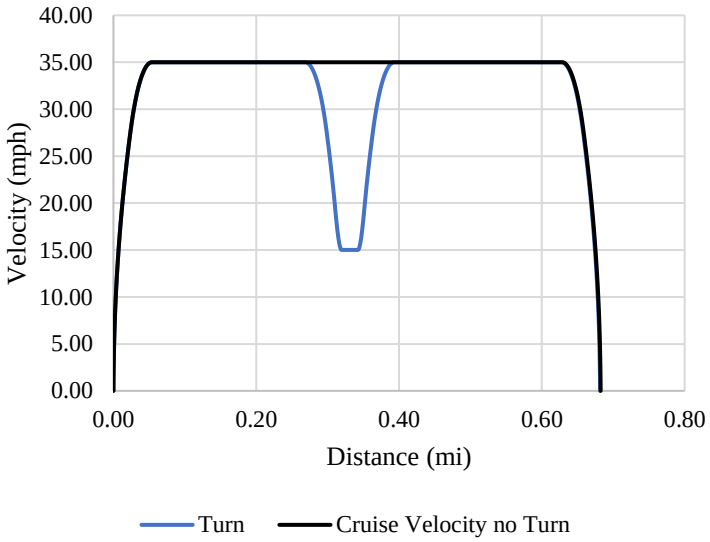

Figure 3-17: Velocity profile as a function of distance for a one-turn synthesized route.

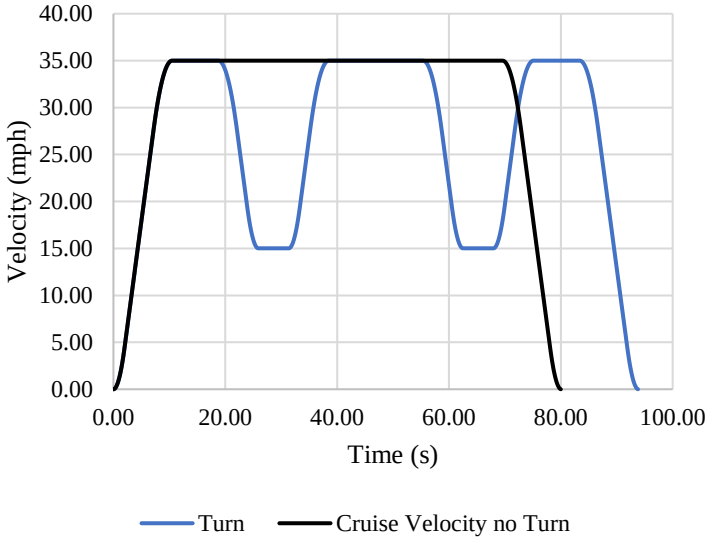

Figure 3-18: Velocity profile as a function of time for a two-turn synthesized route.

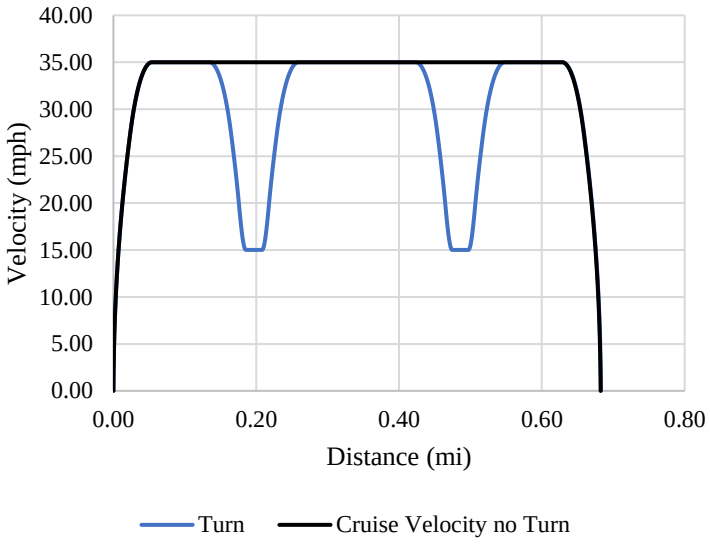

Figure 3-19: Velocity profile as a function of distance for a two-turn synthesized route.

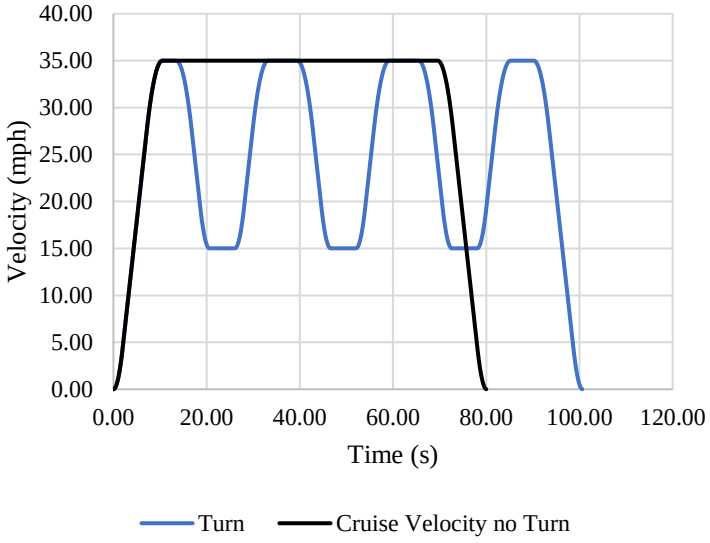

Figure 3-20: Velocity profile as a function of time for a three-turn synthesized route.

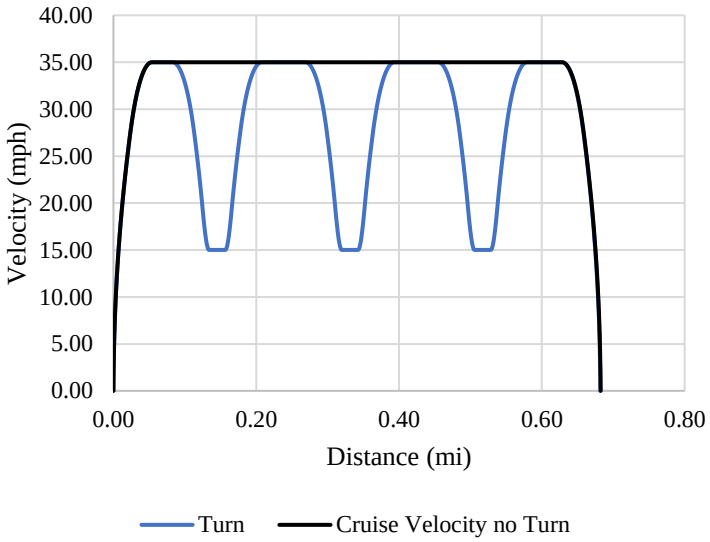

Figure 3-21: Velocity profile as a function of distance for a three-turn synthesized route.

The energy consumption results of the above turn iterations are shown in Table 3-5. With each additional curve, the route energy consumption increases, on average, 7.2 DC Wh/mi, and the route travel time increases by 6.9 seconds. The consistent increase in consumption and time indicates that the penalties associated with corners are predictable by knowing the curve properties and the lateral accelerations at which they will be navigated.

Table 3-5: Route energy consumption and time results of systematic turn additions.

Turns	**DC Wh/mi**	**Δ DC Wh/mi per iteration**	**Time (s)**	**Δ Time with previous iteration**
0 (Cruise Profile)	226.3	-	80	-
1	233.6	7.3	86.8	6.8
2	240.6	7	93.8	7
3	247.9	7.3	100.6	6.8
Average increase per turn		**7.2**		**6.9**

Ideal curve look-up table implementation for evaluating the route energy consumption is the block diagram in Figure 3-22. First an origin-destination pair is used to generate a straight-line velocity profile that discounts road curves similar to the work by [3.10]. The resulting profile is used in conjunction with a powertrain model to determine the preliminary pre-curve route energy consumption. The road curves and their corresponding properties along the route are identified using GPS analysis, and they are matched to similar curves in a look-up table to determine the time and energy consumption penalty associated with each one. The curve penalties are totaled and then combined with the straight-road travel time and energy consumption. This reduces the complexity of the route generation process. The significant turns along the route are identified and matched with similar turns in the look-up table to find the associated estimated energy consumption and time penalties. With the results of this case study showing promise, more investigation into other turning situations (i.e. larger or smaller radius, different cruise speeds, different turn intensities) will aid in development of a curve penalty look-up table for use in eco-routing applications.

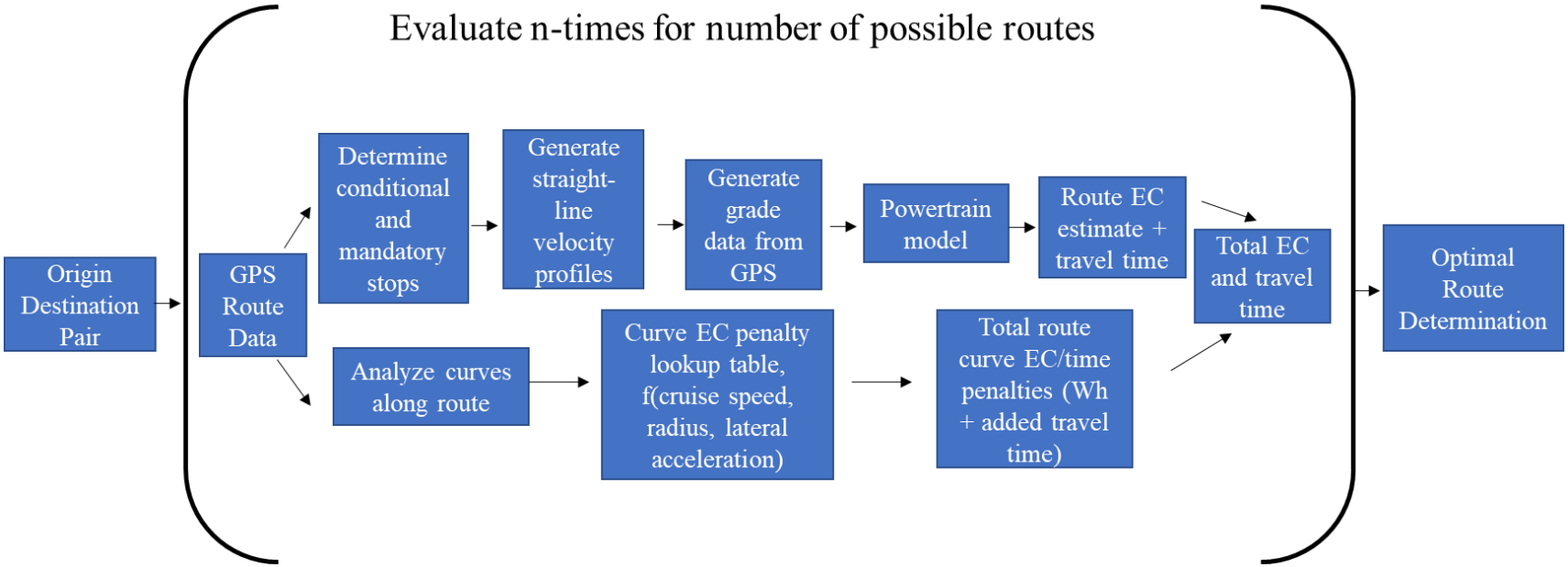

Figure 3-22: Block diagram describing curve look-up table method implementation.

3.5 9 and 7 Region Curve Models

There are two piecewise models considered for synthesizing a curve velocity profile: a 7-region and a 9-region model. The main difference between these two models is when the cornering event, or steering input, begins. The 9-region model initiates the cornering event after the vehicle fully decelerates to the cornering velocity. The 7-region model initiates the cornering before the vehicle has fully decelerated. The resulting velocity and curvature profile of the 7-region model is shown in Figure 3-23, while the experienced lateral, longitudinal, and resultant accelerations are shown in Figure 2-9. The area between the red dotted lines in Figure 3-23 indicate when the vehicle is cornering. The decelerating and accelerating events occur while the vehicle is entering or exiting the corner. The 7-region model is more representative of how the average driver behaves as they execute a cornering maneuver. Tables 3-6, 3-7, and 3-8 are the equations that govern the 7-region model. The 9-region model is how a driver *should* navigate a corner, as combining longitudinal and lateral acceleration events results in a non-zero snap. As mentioned in the journal paper, a non-zero snap is uncomfortable for the occupants and results in unpredictable tire behavior. Figure 3-24 is the 9-region velocity and curvature over the event and Figure 2-8 is the experienced lateral, longitudinal, and resultant accelerations. The red dotted lines indicate the vehicle fully decelerates before entering the curve, and it completes the curve before accelerating back to cruise velocity. Tables 3-9, 3-10, and 3-11 are the equations that govern the 9-region curve model used in this thesis.

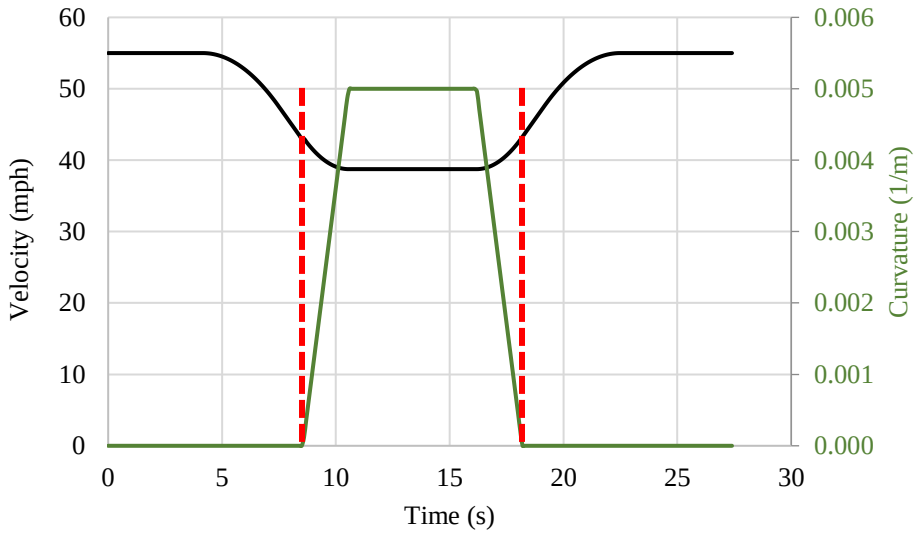

Figure 3-23: Curvature and velocity versus time for the 7-region curve model. Note the cornering begins before the vehicle has fully decelerated to cornering velocity.

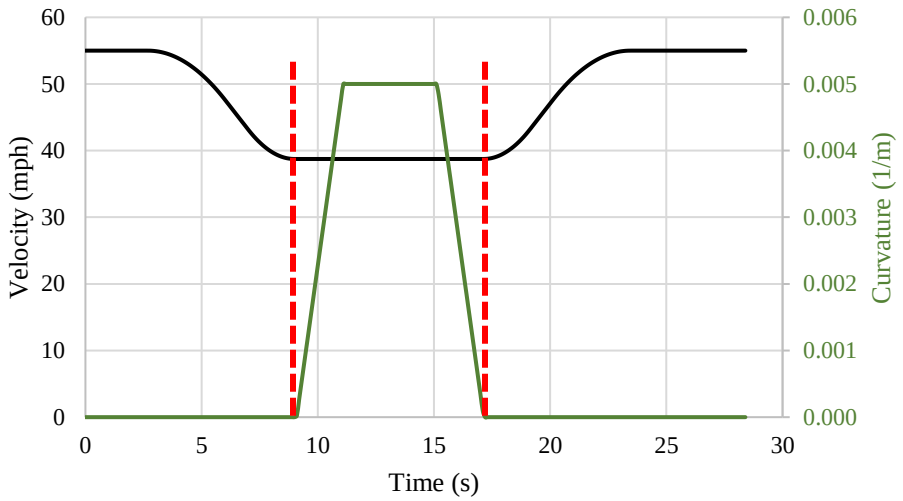

Figure 3-24: Curvature and velocity versus time for the 9-region curve model. Note the cornering does not begin until after the vehicle has fully decelerated to cornering velocity.

Table 3-6: 7-region curve longitudinal variables as a function of region time (shown in Table 3-8)

	Longitudinal			
Region	**Distance** $x(t_r)$	**Velocity** $v(t_r)$	**Acceleration** $a_{long}(t_r)$	**Jerk** $j(t_r)$
1	$\frac{j_{dmax}t_r^3}{6} + v_c t_r$	$\frac{j_{dmax}t_r^2}{2} + v_c$	$j_{dmax}t_r$	j_{dmax}
2	$\frac{d_{max}t_r^2}{2} + v_1 t_r + x_1$	$d_{max}t_r + v_1$	d_{max}	0
3	$\frac{j_{amax}t_r^3}{6} + \frac{d_{max}t_r^2}{2} + v_2 t_r + x_2$	$\frac{j_{amax}t_r^2}{2} + d_{max}t_r + v_2$	$j_{amax}t_r + d_{max}$	j_{amax}
4	$v_t t_r + x_3$	v_t	0	0
5	$\frac{j_{amax}t_r^3}{6} + v_t t_r + x_4$	$\frac{j_{amax}t_r^2}{2} + v_t$	$j_{amax}t_r$	j_{amax}
6	$\frac{a_{max}t_r^2}{2} + v_5 t_r + x_5$	$a_{max}t_r + v_5$	a_{max}	0
7	$\frac{j_{dmax}t_r^3}{6} + \frac{a_{max}t_r^2}{2} + v_6 t_r + x_6$	$\frac{j_{dmax}t_r^2}{2} + a_{max}t_r + v_6$	$j_{dmax}\mathrm{t_r} + a_{max}$	j_{dmax}

Table 3-7: 7-region curve lateral variables as a function of region time (shown in Table 3-8).

Lateral				
Region	**Radians**	**Acceleration**	**Curvature**	**Curvature Rate**
	$\theta(t_r)$	$a_{lat}(t_r)$	$\mathrm{k}(t_r)$	$\dot{k}(t_r)$
1 2	0	0	0	0
3	$\frac{v_t E_r t_r^2}{2}$	$v_t^2 E_r t_r$	$E_r t_r$	E_r
4	$v_t k t_r + \theta_3$	$v_t^2 k$	k	0
5	$\theta_4 + \frac{v_t E_r t_r^2}{2}$	$v_t^2 k - v_t^2 E_r t_r$	$k - E_r t_r$	E_r
6 7	θ_5	0	0	0

Table 3-8: 7-region equations for time delta in each region.

Region	$\boldsymbol{\Delta t_n}$
1	$\frac{d_{max}}{j_{dmax}}$
2	$\frac{-(v_c - v_t)}{d_{max}} - \frac{d_{max}}{2j_{dmax}} + \frac{d_{max}}{2j_{amax}}$
3	$\frac{-d_{max}}{j_{amax}}$
4	$\frac{\theta_t - v_t E_r t_3^2}{v_t k}$
5	$\frac{a_{max}}{j_{amax}}$
6	$\frac{(v_c - v_t)}{a_{max}} - \frac{a_{max}}{2j_{amax}} + \frac{a_{max}}{2j_{dmax}}$
7	$\frac{a_{max}}{j_{dmax}}$

Table 3-9: 9-region curve longitudinal variables as a function of region time (shown in Table 3-11).

Longitudinal				
Region	**Distance** $x(t_r)$	**Velocity** $v(t_r)$	**Acceleration** $a_{long}(t_r)$	**Jerk** $j(t_r)$
1	$\frac{j_{dmax}t_r^3}{6} + v_c t_r$	$\frac{j_{dmax}t_r^2}{2} + v_c$	$j_{dmax}t_r$	j_{dmax}
2	$\frac{d_{max}t_r^2}{2} + v_1 t_r + x_1$	$d_{max}t_r + v_1$	d_{max}	0
3	$\frac{j_{amax}t_r^3}{6} + \frac{d_{max}t_r^2}{2} + v_2 t_r + x_2$	$\frac{j_{amax}t_r^2}{2} + d_{max}t_r + v_2$	$j_{amax}t_r + d_{max}$	j_{amax}
4 5 6	$v_t t_r + x_3$	v_t	0	0
7	$\frac{j_{amax}t_r^3}{6} + v_t t_r + x_6$	$\frac{j_{amax}t_r^2}{2} + v_t$	$j_{amax}t_r$	j_{amax}
8	$\frac{a_{max}t_r^2}{2} + v_7 t_r + x_7$	$a_{max}t_r + v_7$	a_{max}	0
9	$\frac{j_{dmax}t_r^3}{6} + \frac{a_{max}t_r^2}{2} + v_8 t_r + x_8$	$\frac{j_{dmax}t_r^2}{2} + a_{max}t_r + v_8$	$j_{dmax}\mathrm{t_r} + a_{max}$	j_{dmax}

Table 3-10: 9-region curve lateral variables as a function of region time (shown in Table 3-11).

Lateral				
Region	**Radians** $\theta(t_r)$	**Acceleration** $a_{lat}(t_r)$	**Curvature** $\mathrm{k}(t_r)$	**Curvature Rate** $\dot{k}(t_r)$
1 2 3	0	0	0	0
4	$\frac{v_t E_r t_r^2}{2}$	$v_t^2 E_r t_r$	$E_r t_r$	E_r
5	$v_t k t_r + \theta_4$	$v_t^2 k$	k	0
6	$\theta_5 + \frac{v_t E_r t_r^2}{2}$	$v_t^2 k - v_t^2 E_r t_r$	$k - E_r t_r$	E_r
7 8 9	θ_6	0	0	0

Table 3-11: 9-region equations for time delta in each region.

Region	Δt_n
1	$\frac{d_{max}}{j_{dmax}}$
2	$\frac{-(v_c - v_t)}{d_{max}} - \frac{d_{max}}{2j_{dmax}} + \frac{d_{max}}{2j_{amax}}$
3	$\frac{-d_{max}}{j_{amax}}$
4	$\frac{k}{E_r}$
5	$\frac{\theta_t - v_t E_r t_4^2}{v_t k}$
6	$\frac{k}{E_r}$
7	$\frac{a_{max}}{j_{amax}}$
8	$\frac{(v_c - v_t)}{a_{max}} - \frac{a_{max}}{2j_{amax}} + \frac{a_{max}}{2j_{dmax}}$
9	$\frac{a_{max}}{j_{dmax}}$

3.6 References for Supplemental Appendices

[3.1] Argonne National Laboratory, "Downloadable Dynamometer Database," 2018, Available: https://www.anl.gov/energy-systems/group/downloadable-dynamometer-database

[3.2] Vorotovic, G., Rakicevic, B., Mitic, S., Stamenkovic, D., "Determination of Cornering Stiffness Through Integration of A Mathematical Model and Real Vehicle Exploitation Parameters," FME Transactions, vol. 41, no. 1, pp. 66-71, July 2012.

[3.3] Stone, R. and Ball, J., "Automotive Engineering Fundamentals," SAE, ISBN: 0-7680-0987-1, 2004

[3.4] Rajamani, R., "Vehicle Dynamics and Control," Springer, ISBN: 978-1-4614-1432-2, 2012

[3.5] Olofson, H., "Rolling resistance during cornering – impact of lateral forces for heavy-duty vehicles," M.S. Thesis, KTH Royal Institute of Technology, Stockholm, Sweden, 2015.

[3.6] White, E., Nelson, D., and Manning, C., "An Illustrative Look at Energy Flow through Hybrid Powertrains for Design and Analysis," SAE Technical Paper, 14. http://doi.org/10.4271/2015-01-1231, 2015

[3.7] Tamaro, C., "Vehicle powertrain model to predict energy consumption for ecorouting purposes," M.S. Thesis, Dept. Mech. Eng., Virginia Tech, Blacksburg, VA, 2016.

[3.8] Dixon, G., Stobart, R., and Steffen, T., "Unified backwards facing and forwards facing simulation of a hybrid electric vehicle using MATLAB Simscape," SAE Technical Paper 2015-01-1215, doi:10.4271/2015-01-1215, 2015.

[3.9] Idaho National Laboratory, "2013 Chevrolet Volt Advanced Vehicle Testing – Baseline Testing Results," 2014, Available: https://energy.gov/sites/prod/files/2014/02/f7/2013_chevrolet_volt_fs.pdf